Electronic Thesis and Dissertation Repository

4-10-2015 12:00 AM

Non-invasive Quantification of Alveolar Morphometry Measurements in Older Never-smokers

Gregory A. Paulin, *The University of Western Ontario*

Supervisor: Dr. Grace Parraga, *The University of Western Ontario*
A thesis submitted in partial fulfillment of the requirements for the Master of Science degree in Medical Biophysics
© Gregory A. Paulin 2015

Follow this and additional works at: https://ir.lib.uwo.ca/etd

⚙ Part of the Investigative Techniques Commons, Medical Biophysics Commons, Respiratory System Commons, and the Respiratory Tract Diseases Commons

NON-INVASIVE QUANTIFICATION OF ALVEOLAR MORPHOMETRY
MEASUREMENTS IN OLDER NEVER-SMOKERS

(Thesis format: Integrated Article)

by

Gregory <u>Paulin</u>

Graduate Program in Medical Biophysics

A thesis submitted in partial fulfillment
of the requirements for the degree of
Master of Science

The School of Graduate and Postdoctoral Studies
The University of Western Ontario
London, Ontario, Canada

© Gregory Paulin 2015
THE UNIVERSITY OF WESTERN ONTARIO

Abstract

Diffusion-weighted noble gas pulmonary magnetic resonance imaging (MRI) provides *in vivo* images with a contrast uniquely sensitive to molecular displacement at cellular and sub-cellular length scales. We estimated the external airway radius (R) and internal airway radius (r) of the alveolar dimensions to evaluate potential differences in acinar duct morphometries in healthy older never-smokers and compared those with a group of ex-smokers. The acinar duct and alveolar MRI morphometry results were within the physiologically-valid range of parameters. Estimated values of internal (r) and external (R) airway radius as well as alveolar sheath (h) and mean linear intercept (L_m) for individual subjects were similar with low variance. Results showed that MRI measurements of lung air space size in healthy older never-smokers were elevated compared to previous results reported in younger never-smokers, and lower than in age-matched ex-smokers ($p<.05$). Specifically, older never-smokers had significantly lower external and internal airway radius and mean linear intercept, but higher alveolar sheath thickness, alveolar density and surface area-to-volume ratio than ex-smokers ($p<.05$). Such results are compatible with the senile emphysematous changes to healthy parenchyma that accompany aging. These results demonstrate the potential MRI has with regards to replacing histology and lung stereology as the gold standard for measuring pulmonary acinus microstructure.

Keywords

Co-Authorship Statement

The following thesis contains the basis of an original manuscript submitted for peer review to the *Journal of Applied Physiology* entitled "Non-invasive Quantification of Alveolar Morphometry in Older never-smokers". The manuscript was co-authored by Gregory Paulin, Alexei Ouriadov, Khadija Sheikh, David G. McCormack and Grace Parraga.

As the principal author and M.Sc. candidate, Gregory Paulin booked and consented patients, led study subject visits, performed pulmonary function tests, acquired MR and CT images, collaborated with model software development, processed and analyzed all data, performed statistical analysis, led interpretation of results, and drafted the original manuscript. Alexei Ouriadov led morphometry model development and provided technical expertise. Khadija Sheikh helped with statistical analysis and provided editorial assistance. Dr. David G. McCormack provided technical and clinical expertise. Dr. Grace Parraga, as the principal investigator, led the study design, helped to determine project objectives, provided mentorship, assisted with the interpretation of results, and provided editorial assistance as well as overall guidance throughout the study.

Pulmonary function data acquisition was performed under the supervision of Sandra Blamires, CCRC. Hyperpolarization of ^{3}He gas was performed by Andrew Wheatley, BSc. MRI acquisition was performed by Trevor Szekeres, MRT(MR)(R).

Acknowledgments

I would like to first start off by acknowledging my supervisor, Dr. Grace Parraga, for her guidance, wisdom, and expertise throughout my master's education. Her patience, dedication and constant motivation over the last two years has been invaluable to me during my time working in her incredible research group. I am incredibly grateful for the opportunities she has given me, and am sincerely appreciative of the wealth of hands-on patient interaction I was able to experience while a member of her lab. I value the knowledge I have gleaned during my time here, and aim to apply what I have learned to all of my future endeavours. I would also like to thank the members of my advisory committee, Dr. James Lewis and Dr. Hanif Ladak, for their input, support, and advice during my graduate career.

I gratefully acknowledge the financial support I have received from the province of Ontario in the form of an Ontario Graduate Scholarship (OGS), as well as the Western Graduate Research Stipend (WGRS).

I would like to thank the staff of the Parraga lab, most notably Andrew Wheatley, Sandra Blamires, Alexei Ouriadov and Trevor Szekeres. To Andrew, thank you for all the technical support; your skill with the polarizer made sure that each subject visit went smoothly and without fail. To Sandra, thank you for all the time you spent training me with PFT's, and for always being there to support me even during the most difficult of patient visits. To Alexei, I would like to thank you for your patience and willingness to help me when trying to decipher even the most technical and challenging aspects of my project. To Trevor, thank you for so expertly performing the numerous ^{3}He MRI scans I required, without which this work would not have been possible.

To my lab-mates, I would like to acknowledge your incredible friendship and support over these past two years. Together, you helped me to persevere through the toughest of times, and helped me enjoy and appreciate the good times that much more. To Sarah, thank you for being there for me on my first day, training me with ^{3}He MRI segmentation and working with me on my first publication in the lab. To Khadija, I cannot thank you enough for all

Table of Contents

List of Tables

List of Figures

List of Appendices

List of Abbreviations

ADC	Apparent Diffusion Coefficient
BMI	Body Mass Index
CO_2	Carbon Dioxide
COPD	Chronic Obstructive Pulmonary Disease
CT	Computed Tomography
CPET	Cardiopulmonary Exercise Test Measurements
$\overline{D}$	Mean Diffusion Coefficient
$\overline{D}_{an}$	Anisotropic Diffusion Coefficient
D_L	Longitudinal Diffusion Coefficient
D_T	Transverse Diffusion Coefficient
D_0	Free Diffusion Coefficient
DL_{CO}	Diffusion Capacity of the Lung for Carbon Monoxide
FEV_1	Forced Expiratory Volume in 1 Second
FRC	Functional Residual Capacity
GOLD	Global Initiative for Obstructive Lung Disease
h	Alveolar Sheath Depth
HU	Hounsfield Unit
^3He	Helium-3
L	Alveolar Length
L_m	Mean Linear Intercept
MRI	Magnetic Resonance Imaging
N_a	Alveolar Density
O_2	Oxygen
PFT	Pulmonary Function Test
R	External Airway Radius
r	Internal Airway Radius
RA_{950}	Relative Area with Attenuation Values Below -950HU
RV	Residual Volume
S/V	Surface Area to Volume Ratio

TE	Echo Time
TR	Repetition Time
TLC	Total Lung Capacity
UTE	Ultra-short Echo Time
VC	Vital Capacity
VDP	Ventilation Defect Percent
^{129}Xe	Xenon-129

1   CHAPTER 1: INTRODUCTION

The senile lung can be characterized by a homogeneous enlargement of the alveolar airspaces, without fibrosis or destruction of the alveolar walls. The objective of this chapter is to provide an introduction to lung aging and the senile lung, as well as to provide an overview of the historical and current techniques employed for measuring lung morphometry.

1.1   Overview and Motivation

Chronic lower respiratory tract disease is the third leading cause of death in people aged 65 years and older.[1] This disease, comprised of asthma, emphysema, chronic bronchitis, bronchiectasis and chronic obstructive pulmonary disease (COPD), is more prevalent now than ever before as a result of an ever-growing and aging population. With respect to current demographic trends in North America, an understanding of how the body changes with age and how this impacts the respiratory system is critical in order to improve the quality of life of individuals as they approach old age. Moreover, this knowledge is essential for reducing the potentially overwhelming burden that these respiratory diseases place on the currently strained healthcare system.

As individuals age, a variety of structural and functional changes occur, including, but not limited to, a reduction in maximal vital capacity and gas exchange, as well as a weakening of the respiratory muscles and a deterioration of lung defense mechanisms.[2-6] As detrimental as the aforementioned issues may sound however, these age-related changes rarely present with symptoms on their own. It is true that these changes contribute to an older person's reduced ability to do vigorous exercise, but more often than not, the limiting factor for undertaking strenuous activities are age-related decreases in heart function.[7,8] Instead, what is most important when considering the changes associated with lung aging is not the reduction in maximal function, but rather the increased risk that these changes place on older people that make them more vulnerable to respiratory failure and hypoxia.[9,10] Specifically, the risk of developing pneumonia after bacterial or viral infections and the added complications associated with an already weakening set of lungs. The fundamental premise for understanding the effects these changes have on an individual

is that they disturb health through their ability to exacerbate the effects of heart and lung diseases, and further complicate those caused by various environmental hazards such as smoking or pollution.

Current knowledge of the mechanisms that influence pulmonary structure and function with age is very limited. Even more limited is our understanding of the structural changes that take place on the microstructural or alveolar level (the primary area for gas exchange in the human lung).[11] Existing measures of lung morphology are highly invasive, relying predominantly on excised tissue or cadaveric samples. These techniques, such as lung histology and stereology, depend on extensive user input, and as such are prone to subjective bias as a result of opinions on topics such as sample selection or specimen preparation techniques.[12-14] Most importantly, the established techniques cannot provide *in vivo*, individualized information on the nature of lung aging as it is taking place in the body. Currently, the microstructural changes observed in the aging lung are referred to as senile emphysema, and is characterized by an enlargement of the alveolar space without fibrosis or tissue destruction.[3] Unfortunately, there is limited information regarding the nature or etiology of these changes, as well as their effect on quality of life. Thus, in order to combat the impending pulmonary challenges of an aging population, non-invasive, reproducible, and accurate methods for measuring lung microstructure are essential in furthering our understanding of pulmonary development and deterioration.

This thesis focuses on the development and application of a direct, non-invasive quantitative measurement of alveolar morphometry derived from hyperpolarized helium-3 (^{3}He) diffusion-weighted magnetic resonance imaging (MRI) in a group of older never-smokers. This chapter reviews the literature regarding the anatomy of the human lung and the physiological changes which occur with normal aging. Specifically, this section will focus on the structural and functional changes that occur in the aging human lung, with an emphasis on the nature of senile emphysema as it compares to COPD-related emphysema. A survey of current lung morphometric tools is also included, with a look at the current gold standard lung stereology, as well as two more novel techniques consisting of high-resolution X-ray micro-computed tomography (micro-CT) and hyperpolarized ^{3}He diffusion MRI. Lastly, an overview of the hypotheses tested in this thesis regarding the

nature and etiology of senile emphysema and its connection to COPD-related emphysema are described, along with a summary of the overall objectives of this study.

1.2 The Lung

1.2.1 Anatomy and Microstructure of the Lung

The human lungs, consisting of both a left and right lung, are the essential organs for respiration. The key role of the lungs is to bring oxygen (O_2) into the body, and remove carbon dioxide (CO_2), the primary waste product. Figure 1-1 depicts an overview of the main structures involved in the respiratory system.[15] A double layered serous membrane surrounds each lung, with the outer layer, parietal pleura, attached to the wall of the thoracic cavity, and the inner layer, visceral pleura, covering the outside surface of each lung.[16] Between these two layers is a region called the pleural cavity which creates space for the lungs to expand into during inhalation. The entirety of the lungs are enclosed in and protected by the rib cage. The right lung is comprised of three lobes (upper, middle, and lower lobe), while the left lung is slightly smaller, having only two lobes (upper and lower lobe) with an area designated for the heart known as the cardiac notch. The horizontal fissure separates the upper and middle lobes, while the right oblique fissure separates the middle and lower lobes in the right lung. In the left lung, the left oblique fissure separates the upper and lower lobes.[17]
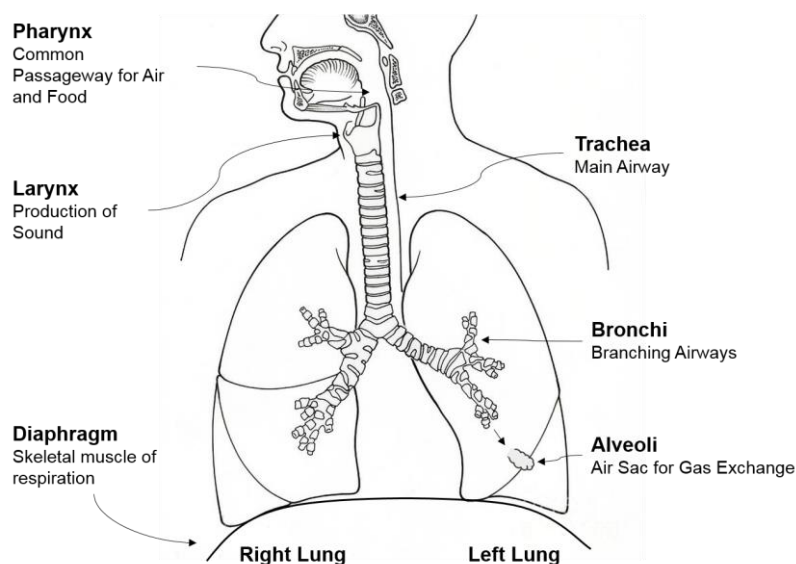
Figure 1-1: The Respiratory System. The biological system responsible for the intake and exchange of oxygen (O_2) and carbon dioxide (CO_2).

Air first enters the body when inhaled through the nose or mouth. From here, it travels through the pharynx and larynx, where it eventually reaches the trachea. The trachea splits into the left and right primary bronchus which feed each lung independently. These bronchi can be described as large hollow tubes which are kept rigid by a series of cartilaginous rings to prevent collapse and/or blockage of airflow to the lungs. The main bronchi branch off into secondary bronchi which feed each lobe, and then into tertiary bronchi within each lobe.[15] Mucus is secreted onto bronchial surfaces via goblet cells which line the inner surface of these bronchi.[18] Ciliated columnar cells are also present and function together to push mucus secreted by goblet cells out of the lungs. This cooperative mechanism, known as the mucociliary elevator, enables the lungs to clear away dust, pathogens, viruses, bacteria and fungi from the respiratory tract, trapping the contaminants in mucus which are then carried by the cilia to the mouth where it is eventually swallowed or coughed up.[2,19]

Numerous small bronchioles branch off from the tertiary bronchi in each lobe. These bronchioles differ from the preceding bronchi in part due to their smaller size, but most significantly in the composition of their inner walls. These airways lack the stiff hyaline cartilage rings found in bronchi, and are instead comprised of elastin fibers and smooth muscle tissue.[20] These characteristics enable the bronchioles to change their diameter significantly in response to biological need, such as dilation during exercise or constriction when exposed to environmental pollutants. The bronchioles continues to branch until they become what are commonly known as terminal bronchioles which are located beginning around the 16th generation (Figure 1-2).[20,21] These bronchioles are amongst the smallest in the lungs and terminate at the alveoli, signaling the end of what is known as the conducting zone of the lung, compromised of the trachea, bronchi and conducting bronchioles.

				Generation
Conducting Airways	Trachea	Cartilage, Bronchial Glands		
				0
	Bronchi			1
				2
				↓
				7
	Bronchioles	Non-respiratory		8
				9
				↓
				15
Terminal Respiratory Units		Respiratory		16
				17
				18
				19
	Alveolar Ducts			20
				21
				22
				23
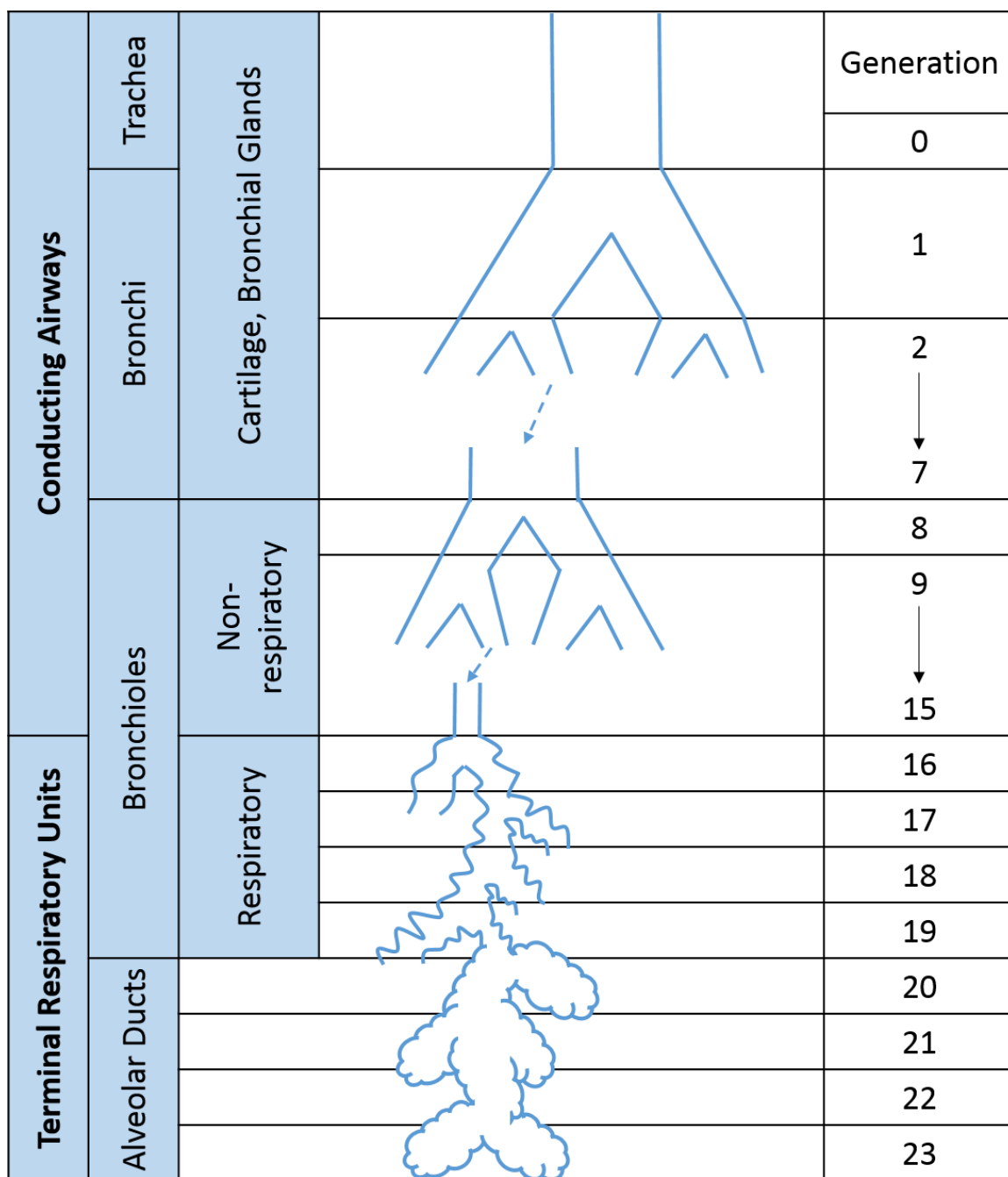
Figure 1-2: Human Airway Tree. Schematic of the human airway tree including the conducting and respiratory zones.

Beginning around the 17th generation are the respiratory bronchioles, named as such due to the alveoli which line their walls. Alveoli, the functional units of the lung, appear as small hollow cavities, which permit gas exchange between air in the lungs and the blood in the local capillaries (Figure 1-3).[22,23] Inhaled O_2 and exhaled CO_2 diffuse between the

alveolar space and local capillaries as a result of a steep concentration gradient which is maintained by a combination of constant breathing and continuous blood flow in the capillaries.[24] Three major cell types make up the alveolar wall; Type I squamous alveolar cells form the main structure of the alveolar wall, while Type II great alveolar cells secrete pulmonary surfactant to aid in inflation of the alveoli, and lastly macrophages which function to capture and phagocytize pathogens and other foreign material.[25,26] By the 20th generation, the entire airway is lined with alveoli, and these bronchioles are now referred to as alveolar ducts. These ducts end around the 23rd generation in sacs lined with alveoli and are consequently referred to as the alveolar sacs. The lungs contain approximately 300-500 million alveoli, with a total surface area ranging from 50-100 square meters (roughly the same size as an outdoor tennis court).[22,27]
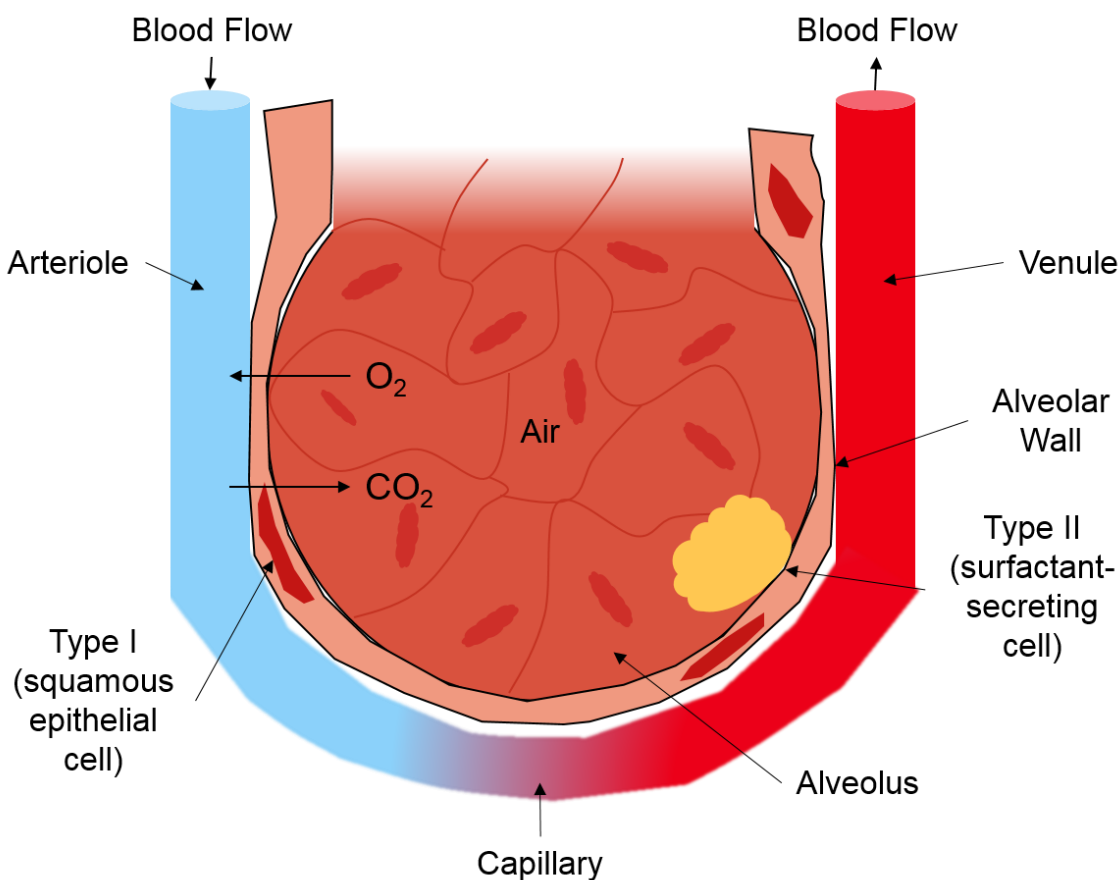
Figure 1-3: Alveoli and Gas Exchange. Alveolar cellular composition and structure. Total surface area available for gas exchange can range from anywhere between 50-100m^2.

1.2.2   Lung Function

Efficient ventilation of the lungs relies on the concerted efforts of the diaphragm and both the external and internal intercostal muscles. This ventilation depends on the process of negative pressure breathing which requires a pressure differential between atmospheric air and that inside the alveoli.[28] To accomplish this, muscles surrounding the lung expand and contract to change the volume of the thoracic cavity. Inhalation (or inspiration) depends on the active expansion of the thoracic cavity, in which there is contraction of both the diaphragm and external intercostal muscles. These changes effectively lower intrathoracic pressure while increasing intraabdominal pressure, ultimately drawing atmospheric air into the lungs by raising the rib cage and moving the abdominal contents downwards and outwards.[20,26] In contrast to inhalation, exhalation is a predominantly passive process, relying on the elasticity of pulmonary tissues to reduce the thoracic cavity size and expel air from the lungs, with the assistance of the internal intercostal muscles during deep exhalation.[29]

Total lung capacity (TLC) of a typical adult human is between 4-6 litres, with variations depending on the combined effects of height, age, gender, and respiratory health.[30,31] Figure 1-4 shows standard lung volumes resulting from normal and forced respiration. The average human respiratory rate is 12-20 breath per minute.[32] With each breath, approximately 0.5 litres of air is moved into or out of the lungs, referred to as the tidal volume, which equates to roughly 6-10 litres of air exchanged per minute.[11,32] A resting midpoint of the lungs is achieved when the inward elastic force reaches equilibrium with the outward force of the thorax. This volume (approximately 2-3 litres in an average young adult) is consistent with the functional residual capacity (FRC) of the lungs, and is the volume of air present at the end of a normal tidal breath. During forced inhalation/exhalation, or what is known as deep breathing, the volume of air exchanged with each breath can reach anywhere from 3 to 5 litres, also known as the vital capacity (VC) of the lungs.[33,34] Regardless of the forcefulness of breathing, there remains at all times approximately 1 litre of air in the lungs, referred to as the residual volume (RV).[33]
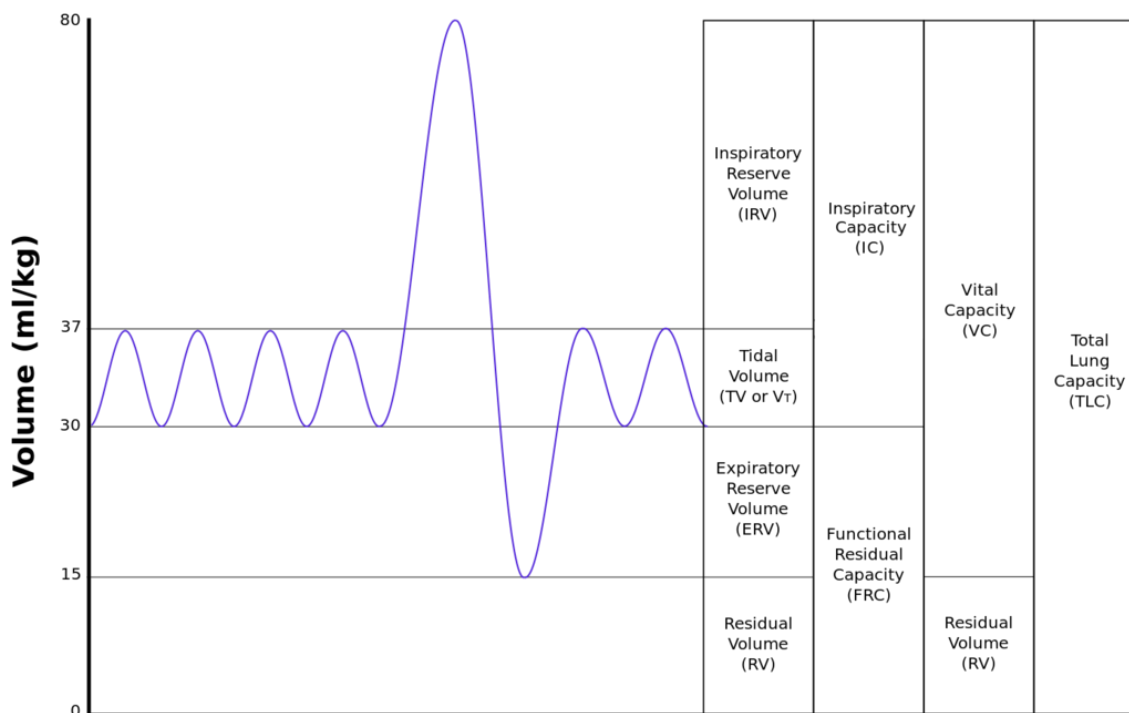
Figure 1-4: Lung Volumes. Lung volumes of a healthy adult can be measured using plethysmography and include vital capacity, tidal volume, expiratory reserve volume, residual volume, inspiratory reserve volume, functional residual capacity and total lung volume.

1.3   Lung Aging

1.3.1   Structural Changes

The lungs undergo significant and crucial developmental changes over the first two decades of life. By the age of 12, the maximal number of alveoli has been reached, and over the following decade the respiratory system rapidly approaches optimal functional capacity. Unfortunately, after this period of accelerated growth (25 years for males, 20 years for females), the lungs begin a progressive decline in performance until death.[35] The major physiological changes that occur in the aging respiratory system may reflect several mechanistic/structural changes such as: 1) diminished lung elasticity; 2) increased stiffness of the chest wall; 3) a reduction in respiratory muscle strength; and 4) an overall change in the shape and structure of the lung.[5,36,37]

Specifically, previous work by Knudson et al showed that there was decreased lung elasticity with age in a group of never-smokers, aged 25-75.[38] The cause of these changes

is not well established since the concentrations of elastin and collagen do not change with age. Specifically, lung elastin remains relatively stable over time, with a typical longevity approaching decades.[39] The reduced elastic recoil and diffusing capacity of the lung (a measure of the transfer of gas from the lungs to the surrounding blood vessels) is believed to be a result of stress relaxation of elastin-fibers as evidenced by an apparent increase in thickness along with the appearance of more loosely associated fibers.[40] A disruption in collagen fibers leading to an increase in intermolecular crosslinks has also been postulated to result in diminished elastic recoil; however there is limited and conflicting evidence to support this theory at present.[41]

Another factor contributing to the deterioration of lung function with age is decreased chest wall compliance. As the body ages, the rib cage along with various associated points of articulations experience calcification resulting in increased stiffening.[3,42] Additionally, osteoporosis can also lead to changes in the shape of the thorax, resulting in a phenotype commonly known as a "barrel chest". The changes in chest wall compliance along with the kyphotic curvature of the spine with age both contribute to the deformation of the diaphragm leading to a reduction in its force-generating capabilities.[5,42] The general reduction in overall muscle mass, specifically type II fast twitch fibers, as well as a loss of peripheral motor neurons and corresponding alterations in neuromuscular junctions also contributes to a significant reduction in respiratory muscle strength.[43]

With regard to lung development and maturation, the large airways remain relatively stable in terms of abundance and diameter. Smaller airways however begin to narrow, and there is actually a loss in the number of total airways present in the lung.[44] The disappearance of smaller airways appears related to a loss of supporting connective tissue which results in frequent collapse of weakened alveolar ducts.[3] A number of structural changes occur within the aging alveoli as well. Studies have shown that the average distance between airspace walls increases (L_m, mean linear intercept) and alveolar pores become much larger[45], while the alveoli themselves become much shallower.[3] These changes are also associated with an increase in alveolar septal thickness, leading to a uniform pattern of airspace dilation and overall reduction in total lung surface area.[46]

1.3.2 Functional Changes

The underlying structural changes that occur in the aging lung affect all levels of lung function, including dynamic flow rates, static lung volumes and alveolar gas exchange rates. Most of what is known regarding changes in lung function with age comes from cross-sectional studies which rely on pulmonary function tests (PFTs). Our current understanding of lung function decline with aging stems from work done by Fletcher et al in 1977. This work showed a continuous decline in the forced expiratory volume in 1 second (FEV_1) at a rate of roughly 42 ml/yr beginning between the ages of 25 and 30 (Figure 1-5).[47] Various more recent longitudinal cross-sectional studies have validated these findings and shown that the rate of loss is greater in males than in females.[42] Additionally, forced vital capacity (FVC) has been shown to steadily decrease to around 75% of peak-value. Together with the age-related changes in FEV_1, this results in an overall decrease in the FEV_1/FVC ratio to around 70-75% by the age of 70, as FEV_1 declines more rapidly than FVC.[48,49]
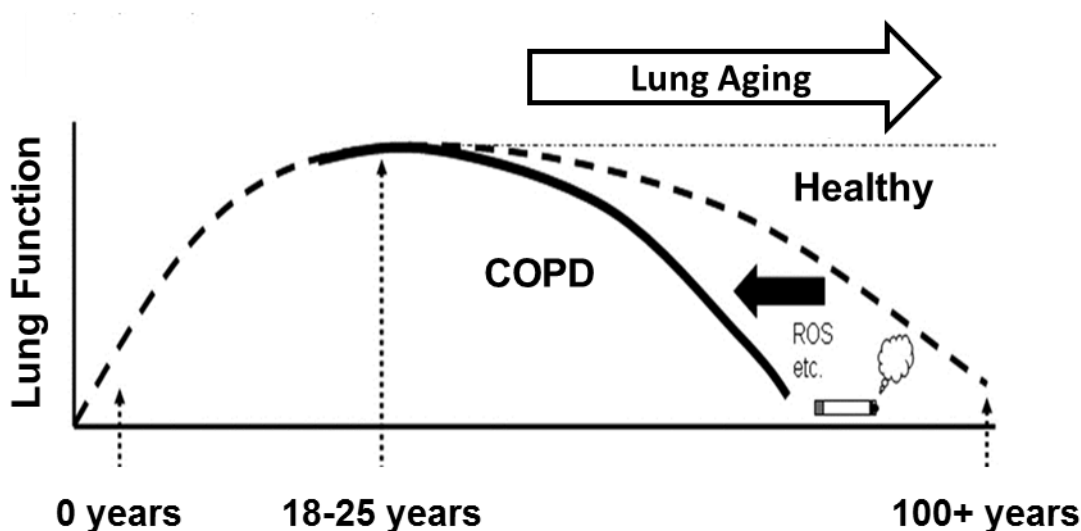
Figure 1-5: Pulmonary Function Declines in Normal Aging and COPD. Lung function declines in COPD hypothesized as an accelerated form of aging. Adapted from work by Fletcher & Peto and Ito & Barnes.[47,50]

With regards to static lung volumes, the age-dependent reduction in elastic recoil has been shown to lead to an increase in RV as a result of gas trapping, by approximately 50% up to

the age of 70.[51] The combination of the chest wall becoming less compliant along with lungs becoming more distensible has also been shown to increase FRC. This increase in residual capacity cause older subjects to breath at higher lung volumes than normal which places an additional burden on the respiratory muscles.[52] Studies in elderly subjects have shown that during resting tidal breathing these changes can result in a 20% increase in breathing-related energy expenditure as compared with a 20 year-old subject.[42] Interestingly, TLC does not change significantly with age, as stiffening of the chest wall has been shown to counterbalance the decrease of elastic recoil in the lungs.[5,53]

The diffusing capacity of the lung has also been shown to decrease markedly with age.[54] Recent studies have shown a decline in the diffusing capacity of the lungs for carbon monoxide (DL_{CO}) to values approximately two-thirds of those predicted for otherwise healthy young adults.[53,54] Several factors are thought to explain this drastic drop in diffusing capacity, with the most common theories being a decrease in the efficiency of pulmonary ventilation and a loss of alveolar surface area combined with reduced blood flow in pulmonary capillaries. Studies have shown however that the density of pulmonary capillaries remains unchanged with age, and thus the most significant factor influencing this decline appears to be the reduction of alveolar surface area.[55,56]

1.3.3   Imaging Studies of the Aging Lung

Presently, there is limited literature available in the field of pulmonary imaging of older never-smokers. The majority of studies have predominantly applied non-invasive imaging tools to differentiate ex-smokers with COPD from control groups of older never-smokers. These studies aimed to develop a deeper understanding of lung structure and function of the diseased lung, while ignoring the unique characteristics and traits of the presumably healthy aged lung. A number of reasons may exist for the lack of data in older subjects, with one explanation being the added difficulty in working with elderly patients as opposed to younger subjects. Specifically, simple positioning of the patient requires more time, and often patients need assistance and increased supervision.[57] This need for more time and staff limits the practicality of research in the elderly. In addition to these constraints, age-related factors such as poor renal function limit the use of many contrast agents when performing computed tomography (CT) or MRI, due to the increased risk of nephrogenic

systemic fibrosis.[58] Further complicating matters are the presence of contra-indicators such as cardiac pace makers or older ferromagnetic surgical material which severely restrict the use of imaging techniques such as MRI.[57]

When studying the elderly, it is especially important to separate the normal process of aging from the presence of disease itself. In some cases, differentiation may not be possible without extensive imaging or invasive procedures. Normative structural or functional values are sparse or not well described in the literature, with age-related changes in airspace size and fibrosis typically described as moderate.

One example of the ambiguity regarding normal aging and disease is the common finding of moderate basal lung fibrosis, which may be due to age-related changes or interstitial lung disease.[3,57] A differentiation of these findings is important as it can mean the difference between a specific treatment and a non-interventional approach as would be the case with simple age-related changes. Therefore, close correlation between the morphological extent of the fibrotic changes, clinical history, and observation of associated changes is essential. Another example of the ambiguity between disease and the normal aging occurs in the case of airspace enlargement evident using a number of imaging modalities such as CT and noble gas MRI. The finding of senile emphysema is usually not accompanied by the clinical findings of COPD-linked emphysema, such as breathlessness on exertion, and these difference are further outlined in Chapter 1.3.4.

A recent study by Copley et al. aimed to describe thin-section pulmonary CT features in a group of asymptomatic elderly subjects. Their results showed that there were a large number of elderly asymptomatic adults (> 75 years) with centrilobular emphysematous changes in CT imaging as compared to a younger control group (< 55 years).[59] In the same study, interstitial changes of the lung with a sub-pleural reticular pattern was found in 60% of the elderly patients, which was completely absent in the younger group. Additionally, 25% of the elderly asymptomatic patients showed small cysts. A related study by Lee et al. also using thin-section CT showed an increase in air trapping with age, with a significant proportion of subjects (50%) being asymptomatic.[60]

More recently, a study by Sheikh et al. looked to utilize noble gas MRI to better understand the determinants and physiological consequences of ventilation defects in older never-smokers. To do so, they evaluated pulmonary function and cardiopulmonary exercise test measurements (CPET) in a group of 52 older-never smokers (mean age 71 years). This study represents the first large imaging study of healthy older never-smokers without a history of chronic heart or lung disease. Interestingly, the study found that while a minority of subjects reported occupational exposures, most subjects had visually obvious ventilation defects that were not resolved following administration of salbutamol.[61] The ventilation defects were modest (~5%) and predominantly observed along the periphery of the lung suggesting that terminal airway closure or narrowing may be a normal age-related pulmonary finding. Additionally, there were no differences in CPET or dyspnea measurements between subjects with and without ventilation defects, supporting the notion that cardiovascular, and not respiratory factors, dominate exercise limitations.[8] From these findings, it is evident that there are physiological changes occurring in the aging lung that are poorly understood, and as such would benefit from a more thorough evaluation of pulmonary microstructure.

1.3.4   Senile Emphysema and COPD-related Emphysema

The senile lung can be characterized by a homogeneous enlargement of the alveolar airspaces, without fibrosis or destruction of the alveolar walls. Morphometric studies have shown that in subjects with senile emphysema, there is an increase in the mean linear intercept as well as a decrease in the surface area of airspace wall per unit of lung volume (S/V) as shown in Figure 1-6.[46,52] Classical studies of the age-associated changes in lung structure in 1958 found that these changes only became clinically demonstrable after the age of 80 and were predominantly associated with women.[62] A more recent study by Gillooly and Lamb in 1993 however, found evidence of increased airspace enlargement with age in all subjects.[63] Additionally, there is homogeneous degeneration of the elastic fibers around the alveolar duct starting around the age of 50, as well as reduction in supporting tissue which results in premature closure of small airways during normal breathing and can potentially cause air trapping and hyperinflation.[9,63]
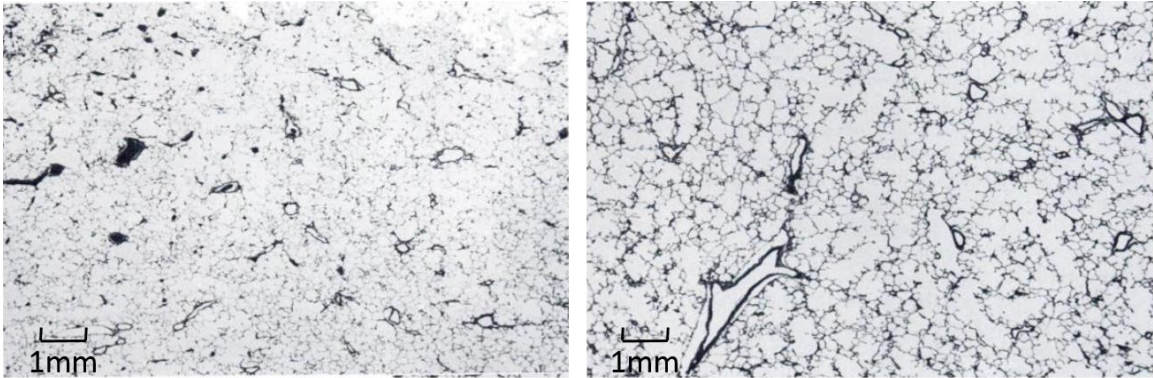
Figure 1-6: Histopathology in Masson Trichrome Stained Human Lung Parenchyma Showing Alveolar Space. Normal lung tissue with L_m=0.279mm (left) and senile lung with L_m=0.532mm (right) at 6x magnification. Adapted with permission.[3]

The term senile emphysema is often considered to be a misnomer, as subjects do not express the symptoms of clinical emphysema, and hence this condition is more correctly referred to as senile lung. Importantly, subjects with senile lung appear to have sufficient lung function for their normal day-to-day activities.[62] These changes do however increase the risk of breathlessness and respiratory failure in the elderly when compromised, and further complicate health when combined with cardiac impairment or respiratory infection.[9,10,64] Specifically, these age-dependent structural and functional changes can reduce sensitivity of the respiratory centres in the presence of hypoxia or hypercapnia, resulting in a diminished ventilatory response in cases of heart failure or aggravated airways obstruction.[5,10,65]

In contrast to the senile lung, emphysema, as first described by Laennec in 1834, is characterized by the dilation and destruction of lung tissue in regions following the terminal bronchioles.[66] In emphysema, the alveoli become deformed, changing into large irregular pockets with reduced surface area for gas exchange with the pulmonary capillaries.[67] Two common forms of emphysema are frequently described in smokers. The first, and most typical form, is called centrilobular emphysema, which is defined by an uneven pattern of tissue destruction predominantly in the upper lobes.[68-70] The second form is known as panlobular emphysema, and is conversely defined by a more homogeneous pattern that is more closely related to genetic disorders as opposed to smoking history or environmental exposures.[69,70] COPD-related emphysema is typically quantified and diagnosed using CT

measures of attenuation. Specifically, this technique uses a cut-off threshold of -950 Hounsfield units for separating emphysematous tissue from normal healthy tissue.[71,72]

It is important to note that current guidelines for COPD based on the Global Initiative for Obstructive Lung Disease (GOLD) lists a post-bronchodilator $FEV_1/FVC < 70\%$ as the threshold for diagnosis of airflow obstruction. The classical epidemiologic studies of Fletcher and Peto demonstrated that death and disability from COPD were related to an accelerated decline in lung function with time, with a loss of 50 to 100 mL in FEV_1 per year, but even in healthy volunteers there is a loss of 20 mL per year with aging resulting in the aforementioned drop in FEV_1/FVC to around 70-75% by the age of 70 (Figure 1-5).[50] In this sense, many subjects will be classified as having airways obstruction by the age of 70 simply as a result of the normal aging process.

Although the changes associated with senile emphysema are histologically different from COPD related emphysema, they result in similar changes in lung compliance and function. A consequence of the reduction in supporting tissues around the airways is a tendency for the smaller airways to collapse. As a result, premature closure of these airways (<2mm) becomes common during normal tidal breathing. Furthermore, the flattening of the internal surface of the alveoli is associated with a reduction in alveolar surface (75 m^2 at age 30 yrs and 60 m^2 at age 70 yrs, ~ -0.27 m^2/yr).[5,42] To date, a number of advanced techniques have been developed and implemented to better measure and visualize pulmonary microstructure. These techniques, which are detailed in the following section, provide an opportunity to better understand the unique changes in alveolar microstructure which occur in the aging lung.

1.4   Techniques for Measuring Lung Morphometry

1.4.1   Lung Stereology

Stereology, the gold standard technique for measuring lung morphometry, is the quantitative characterization of three-dimensional (3D) objects based on measurements made from two-dimensional (2D) cross-sections.[73] One of the defining characteristics of this technique is that it does not depend on any assumptions regarding the shape, size, orientation, or spatial distribution of the object being studied. The technique is founded on

the principles of stochastic geometry and relies on sampling structures with geometric probes.[74,75] The first implementation of these principles occurred in 1843 by mining geologist Delesse who developed a stereological technique to determine volume fraction from area fraction on sections.

Stereology consists of two important stages: sampling and measurement. With regards to sampling, unbiased techniques must be applied at all levels of the analysis. Randomization of both orientation and location of each specimen is also imperative for accurate and precise measurements. The measurements at the final level of sampling are performed using geometric probes as described in Table 1-1. The basic rule is that the dimension of the parameter of interest plus the dimension of the geometric probe used for measurement has to sum to three or greater, according to the values assigned in Table 1-1.[73]

Table 1-1: Relationship of Structural Quantities and Stereological Properties

Parameter	Appearance in 2D Space	Probe	Event	Measurement	Density Estimate
Volume, V_v (3)	Area (2)	Point, P_T (0)	Point lies in volume	Point count, P(x)	$V_v(x)$ $= P(x)/P_T$
Surface Area, S_v (2)	Boundary (1)	Line, L_T (1)	Line intersects surface	Intersection count, I(x)	$S_v(x)$ $= 2 \cdot I(x)/L_T$
Length, L_v (1)	Point (0)	Plane, A_T (2)	Plane transects line	Transect count, Q(x)	$L_v(x)$ $= 2 \cdot Q(x)/A_T$
Number, N_v (0)	-	Volume, P_{T-t} (3)	Dissector volume 'hits' particle top	Top count, Q⁻ (x)	$N_v(x)$ $= Q^-(x)/P_{T-t}$

Stereology has seen use in a broad array of disciplines, from geology (i.e. measuring the fraction of quartz in a rock sample) to medical science (i.e. estimating the total length of capillaries per unit volume of tissue and measuring alveolar density of pulmonary tissue). In fact, the adage that the human lungs have a surface area equivalent to that of an average

tennis court was first derived using stereological methods. Datasets for lung stereology are typically acquired using light or electron microscopy, but can also be collected using other imaging modalities such as immune-electron microscopy,[76] micro-computer tomography[77] and scanning laser optical tomography.[78]

Both the American Thoracic Society (ATS) and the European Respiratory Society (ERS) have defined standards for quantitative assessment of lung morphometry using stereological techniques.[79] Of particular note however, is the use of stereological techniques to measure and assess various forms of pulmonary disease. Emphysema has routinely been studied using stereological techniques such as those shown in Figure 1-7, however most work has ignored the effects of septal destruction, and looked solely at airspace enlargement.[80] Typically this omission is due to the ease in which stereological parameters for airspace enlargement can be acquired. Generally, mean linear intercept (L_m), or mean linear chord length, is used to measure and asses changes in alveolar space. Unfortunately, these parameters can be influenced by various factors such as inflation pressure during fixation and tissue shrinkage after excision. Many morphometric parameters can be easily misinterpreted or skewed if sample preparation is not highly controlled.[81] Loss of elastic recoil, a common physiological change in emphysematous and aging lungs, can further complicate the measurement of airspace size as inflation pressure will have a greater effect on alveolar expansion during specimen fixation. This complication can lead to erroneous evidence of emphysema, even in the absence of disease, as any reduction in the elastic properties of the lung may result in increased airspace volume.[82] Besides the aforementioned inflation related difficulties, serial sectioning of multiple thin slices from tissue specimen is slow, expensive, and can distort the microanatomy. These problems are further exaggerated by fixation techniques which have the potential to alter lung tissue, and denature proteins such as collagen and elastin prior to analysis.
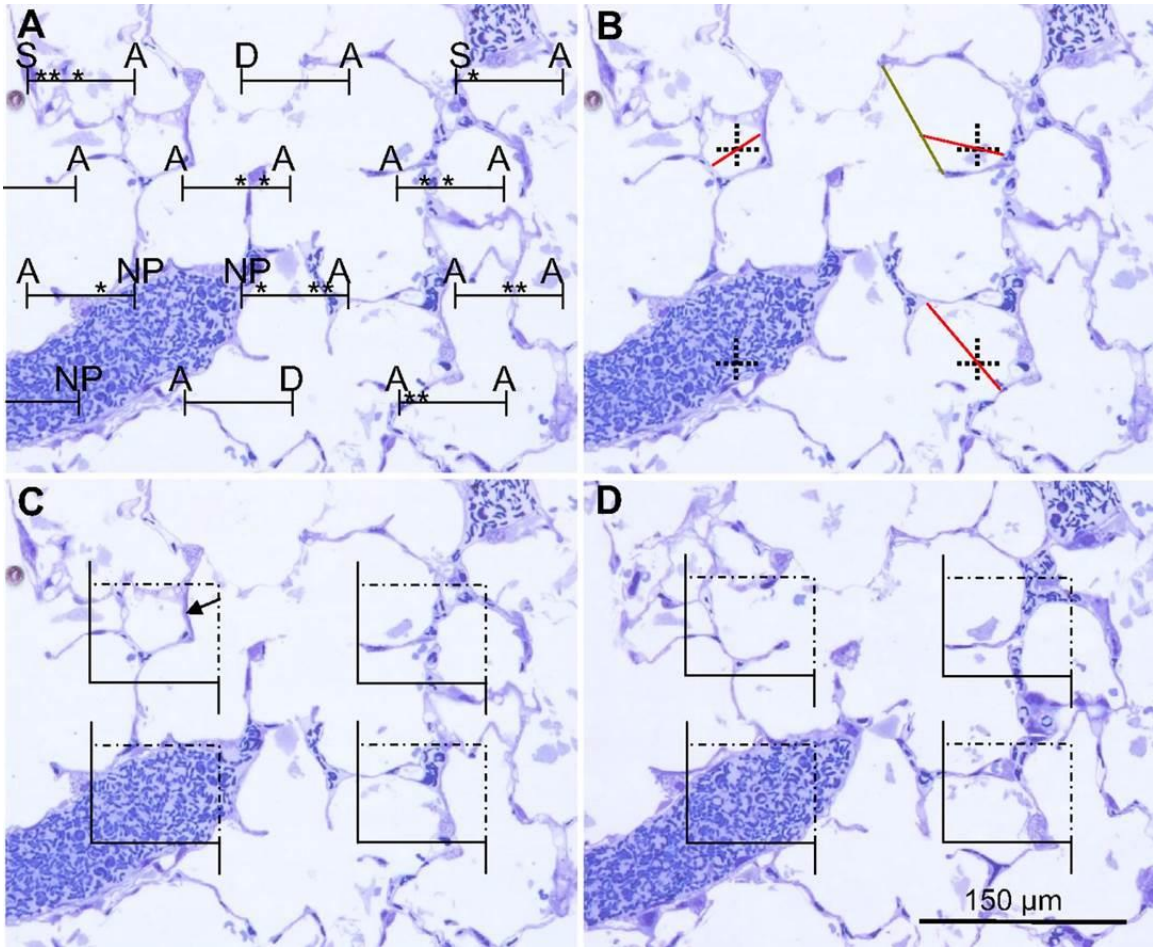
Figure 1-7: Quantitative Assessment of Morphometric Parameters in Emphysema.
A) combined estimation of alveolar luminal (A), ductal airspace (D), and septal (S) volume as well as alveolar septal surface area; B) point-sampled intercepts method; C & D) estimation of the Euler number. Adapted with permission.[82]

1.4.2   High-resolution X-ray Micro-computed Tomography

Since its introduction in the 1970's, x-ray CT has rapidly become the gold standard imaging tool for evaluating pulmonary microstructure. This technique offers the possibility of studying lung microstructure on the basis of the inherent contrast offered by the radio-density differences of tissue structures to air. Briefly, x-ray CT collects a series of image slices compromised of a matrix of pixels (voxels), which are then assigned a specific value (Hounsfield unit; HU) based on the x-ray attenuation signal as compared to that of water.[83,84] Studies of COPD subjects with emphysema agree with histological measurements, presenting evidence of increased airway wall area dimensions[85-87] as well as increased percentage of low attenuation areas.[88,89] Unfortunately, due to the limitation

of standard clinical CT scanners, the smaller airways (<2mm) cannot be resolved. This limitation is quite significant as the small airways are the major site of airflow obstruction in COPD. As such, the applicability of standard CT for measuring alveolar microstructure is quite limited.[71]

Micro–computed tomography (micro-CT) has rapidly emerged as an imaging technique with the potential to measure lung microstructure on length scales much smaller than previously possible with clinical CT scanners. Depending on the x-ray source, focus size, voltage, sample volume, geometric magnification of the optical system, and resolution of the charge-coupled device camera, a spatial resolution of 1-2 μm may be obtained.[90,91] This technology consequently offers the ability to analyze acinar morphometry without the need for physical segmenting, thus maintaining an undamaged, 3D structure.[92]

Recent work by Tsuda et al. and Schittny et al. in 2008 demonstrated the potential of micro-CT to measure alveolar septa in rats[93,94], while its ability to visualize and quantify lung morphometry has also been demonstrated in both mouse[95] and pig models.[96] A number of studies have also recently assessed the practicality of this technique using cadaveric human lung specimens; however, most are conducted with a minimal sample size and/or the omission of any quantitative analysis (Figure 1-8).[97,98]
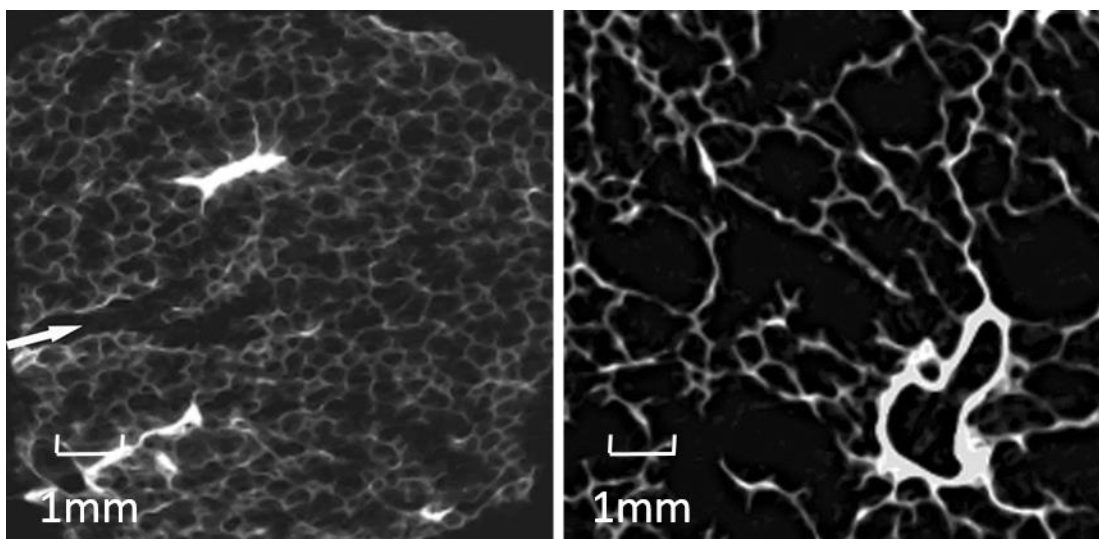
Figure 1-8: Micro-CT of Human Lung Parenchyma. Normal lung parenchyma (left), and centrilobular emphysema (right) showing enlarged alveoli and absent alveolar septa. Field of view is 4mm. Adapted with permission.[97]

With micro-CT imaging, acquiring a complete digital data set of a human lung specimen is now possible. As a non-destructive approach, micro-CT allows analysis of acinar characteristics such as volume, branching, branch length, and surface, over the entire area of interest. Unfortunately, due to the long exposure time and high dose associated with this technique, scanning living organisms is difficult, if not altogether impossible, limiting this modality to use in either *ex vivo* or small animal model studies. When used to study human lungs, the required radiation dose can only be safely applied to isolated lung samples, while the cost of the procedure itself limits its use to only a small number of total specimens. Various inflation and fixation techniques also introduce a variety of error and/or subjective biases when using this technique.[98] Furthermore, when stretching the limits of the system, it can become difficult to determine whether airways with diameters smaller than the achievable resolution are in fact non-existent or simply too narrow to detect via CT.[99] These barriers make micro-CT a highly invasive imaging modality that is unable to capture longitudinal in vivo measurements of the aging lung.

1.5   Measuring Lung Morphometry with MRI

1.5.1   Magnetic Resonance Imaging

MRI relies on the magnetic properties of specific nuclei (most commonly hydrogen protons) in order to create structural or functional images. When these nuclei are placed in a magnetic field and stimulated by radio waves of a particular frequency, they emit radio signals, which can then be used to create an image. Although MRI has a number of advantages over CT, specifically a lack of ionizing radiation and increased soft tissue contrast, the lungs pose a number of unique difficulties for this technique. Since healthy lungs are comprised of 70% air, there is an especially low hydrogen density, making it extremely difficult to acquire any information using conventional proton MRI.[100,101] In addition to this limitation, cardiac and respiratory motion, as well as artifacts resulting from countless air/tissue interfaces hamper the ability of proton MRI to provide novel visual or functional information.[102] Acquiring images under specific breath-hold conditions can help mitigate some of these motion artifacts, however they put severe constraints on image acquisition duration. New proton-based imaging techniques have been designed to help navigate many of these imaging obstacles. One such technique is ultra-short echo time

(UTE) MRI, which limits signal loss in lung parenchyma due to the exceedingly short apparent transverse relaxation time (T2*).[103,104] By utilizing faster pulse sequences that employ shorter echo times (TE), MR images can be acquired with diagnostic quality comparable to that of CT.[105]

1.5.2   Hyperpolarized Noble Gas MRI

Hyperpolarized noble gas MR techniques have been studied for the past two decades, and were first developed in 1994 by Albert et al.[106] This technique relies on the use of either hyperpolarized ^{3}He or ^{129}Xe gas as a contrast agent for functional MR imaging of the lung. ^{3}He, with a gyromagnetic ratio of 32.4MHz/T, has long been the contrast agent of choice, with the potential to provide significant signal intensity after sufficient polarization.

In recent years, ^{3}He MRI has been used to study both pulmonary structure and function in a variety of diseases such as COPD[107-109], asthma[110-112], cystic fibrosis[113-115] and lung cancer[116]. The technique primarily focuses on two major measurements, ventilation defect percent (VDP)[61,117] and apparent diffusion coefficient (ADC).[118-121] In particular, ADC measures helium diffusivity in the lungs due to Brownian motion, with alveoli representing the elementary geometrical unit. The first demonstration of diffusion spectroscopy was performed in 1965 by Stejskal and Tanner.[122] They showed that in the presence of two opposite-polarity gradient pulses, nuclear spins suffer a net phase shift that is proportional to their displacement during the length of the applied pulse plus lobe separation (diffusion time), resulting in a decreased signal amplitude. In the case of free (Gaussian) diffusion (D_0), the MR signal decays according to equation (1):

$$Signal = Signal_0 \exp(-b\, D_0), \tag{1}$$

where *Signal$_0$* is the MR signal intensity in the absence of diffusion-sensitizing gradients. In the presence of internal barriers, such as alveolar walls within the lung, diffusive motion of the gas is restricted and the MR signal decay is described in terms of the ADC as in equation (2):

$$Signal = Signal_0 \exp(-b\, ADC) \tag{2}$$

Unlike the free diffusion scenario, the ADC for restricted diffusion depends on a combination of molecular properties of the gas, tissue structure and shape of the gradient waveform. The b value is proportional to the gyromagnetic ratio of the gas (γ), gradient lobe amplitude (G_m), ramp up/down time (τ), duration of the lobe (δ), and the diffusion time (Δ) according to equation (3)[123,124]:

$$b = (\gamma G_m)^2 \left[\delta^2 \left(\Delta - \frac{\delta}{3} \right) + \tau \left(\delta^2 - 2\Delta\delta + \Delta\tau - \frac{7}{6}\delta\tau + \frac{8}{15}\tau^2 \right) \right] \qquad (3)$$

Studies using this technique have shown that as the lungs age, structural changes occur and result in an annual increase in the ADC of 0.0015cm^2/s for subjects between 20 and 70 years of age from a baseline ADC of 0.20cm^2/s in healthy young adults.[125,126] The ^{3}He ADC technique has also been shown to be highly reproducible[127-129], with a significant correlation with both CT measurements of emphysema[111,130,131] and histological measurements of airspace size.[132] Studies of asymptomatic smokers without COPD have shown elevated ADC measurements, suggesting that the ^{3}He MR technique may provide a sensitive measure of lung tissue destruction before the onset of clinically detectable symptoms.[131,133] Recent studies have developed this technique even further, collecting multiple diffusion weighted images in order to measure geometric parameters (morphometry) within the alveolar space itself.[134-140]

The ^{3}He MR morphometry technique relies on previous work by Weibel and Haefeli-Bleuer who describe the structure of acinar airways as branching trees.[141,142] In this model, the airway tree begins at the trachea, and proceeds through the bronchi and bronchioles to the terminal bronchioles which feed each acinus. Gas ventilation in the conducting airways occurs predominantly by bulk flow (convection), whereas diffusion is the primary mechanism of ventilation beyond the terminal bronchioles in the acinus.[20] The acinus is commonly defined as the largest airway unit in which all airways participate in gas exchange, and represents the complex of all airways distal to the terminal bronchiole, beginning with the primary respiratory bronchioles. A number of studies have adapted and simplified the Weibel model. This adapted model, known as the 'cylinder model', is commonly used in the ^{3}He MR morphometry technique, and describes the airways within

the acinus as cylinders covered by alveolar sleeves, due to the high concentration of alveoli decorating the walls of these airways (Figure 1-9).[134,142-145]
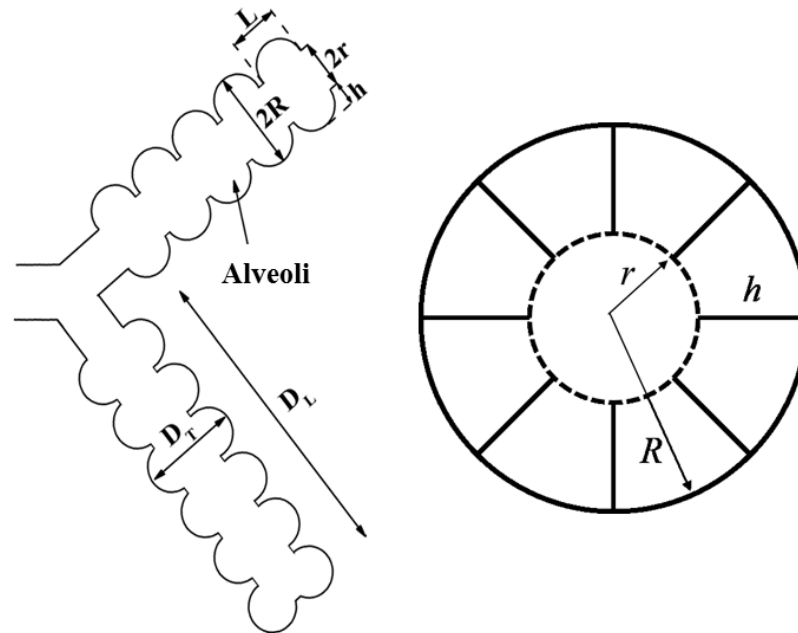
Figure 1-9: Schematic Structure of Two Levels of Acinar Airways. Geometrically, each acinar airway can be considered a cylindrical tube surrounded by an alveolar sleeve. D_T, transverse diffusion; D_L, longitudinal diffusion; L, alveolar length; R, external airway radius; r, internal airway radius; h, alveolar sheath.

The technique for measuring alveolar microstructure was pioneered by Yablonskiy and Sustanskii which considers airways, as opposed to alveoli, as the elementary geometrical units.[134] Diffusion within the airways is anisotropic (direction-dependent), resulting in diffusion rates along and across terminal airways to be independently determined by equation (4)[146]:

$$ADC(\alpha) = (D_L \cos^2 \alpha + D_T \cos^2 \alpha), \tag{4}$$

where α is the angle the principal axis is tilted from the field gradient direction, D_L is the longitudinal diffusion coefficient, and D_T the transverse diffusion coefficient. This angle, α, is crucial as impediments along the airway (longitudinally) are much smaller than those across (transverse). The alveolar walls, ducts, and other branches of the airway tree act as obstacles to the diffusing helium ^{3}He atoms. However, with a spatial resolution in the millimetres currently achievable with ^{3}He MRI, each imaging voxel contains hundreds of

airways of various orientations. Thus, with these limitations, the model assumes that acinar airways are isotropically distributed over a given imaging voxel, and consequently microscopically anisotropic but macroscopically nearly-isotropic.

For each airway, the signal attenuation is exponential with respect to the *b*-value. Due to the dependence of ADC on orientation angle however, the signal decay becomes non-exponential when summing the signal from all airways within a given voxel. Sustanskii and Yablonskiy compare this mathematical problem to that of water diffusion in randomly oriented uniaxial layers as described by Callaghan in 1991.[146] The large number of airways within each voxel allows the orientation distribution function to be assumed uniform, with signal described by equation (5):

$$Signal = Signal_0 \exp(-b\overline{D}) \left(\frac{\pi}{4bD_{an}}\right)^{1/2} \exp\left(\frac{bD_{an}}{3}\right) \Phi\left[(bD_{an})^{1/2}\right] \qquad (5)$$

where $\Phi(x)$ is the error function, and the quantities $\overline{D}$ (mean ADC) and D_{an} (anisotropy of ADC) are described by equations (6) and (7) based on geometrical the characteristics of acinar airways[147]:

$$\overline{D} = \frac{1}{3}D_L + \frac{2}{3}D_T \qquad (6)$$

$$D_{an} = D_L - D_T \qquad (7)$$

It is important to note that when using this technique to measure pulmonary microstructure, the diffusion time must be selected such that the root mean squared diffusion in one direction is larger than the average alveolar radius, but smaller than the mean length of a typical alveolar duct. In doing so, gas atoms are expected to diffuse away from their originating alveoli, yet remain in the same alveolar duct during the duration of the diffusion sensitizing gradient.[140] This constraint recognizes acinar airways, including respiratory broncheoli, alveolar ducts and alveolar sacs, as the elementary geometrical units contributing to the gas diffusion MR signal. Under these conditions, larger conducting bronchioles play little role in the diffusion MR signal formation. Equation (5) assumes that all airways in a given voxel have the same geometric parameters and diffusion coefficients.

As such, in order to minimize the number of parameters, the model assumes that the D_L and D_T for each voxel already represent averaged values.

A detailed description of the ^{3}He MR morphometry procedure is shown in Figure 1-10. Briefly, the technique relies on fitting equations (5), (6), and (7) to multiple b-value measurements of the ^{3}He diffusion-attenuated MR signal which in turn make it possible to evaluate mean geometrical parameters using a number of phenomenological expressions previously derived through Monte Carlo simulations.[147,148] These equations connect D_L and D_T to the characteristic diffusion length in one dimension (L_1) of ^{3}He in the lungs, as well as morphometry parameters of external airway radius (R) and internal airway radius (r) as described in figure 1-9 and equations (8)-(10).

$$L_1 = (2D_0\Delta)^{1/2} \tag{8}$$

$$\frac{D_L}{D_0} = FL\left(bD_0, \frac{r}{R}, \frac{R}{L_1}\right) \tag{9}$$

$$\frac{D_T}{D_0} = FT\left(bD_0, \frac{r}{R}, \frac{R}{L_1}\right) \tag{10}$$

From these values, other physiological parameters can be calculated using equations (11)-(14) from Yablonskiy et al.[135]:

$$L = 2R\sin\frac{\pi}{8} \tag{11}$$

$$S/V = \frac{2\pi R \cdot L + 2\pi \cdot (R^2 - r^2) + 16(R - r) \cdot L}{\pi R^2 L}, \tag{12}$$

$$L_m = 4 \cdot V/S \tag{13}$$

$$N_a = 1/(\pi R^2 L) \tag{14}$$

where L is alveolar length, S/V is the surface area (S)-to-volume (V) ratio of the alveoli, L_m is the mean linear intercept, V/S is the volume (V)-to-surface area (S) ratio, and N_a is alveolar density. Previous studies have shown a close agreement between alveolar

parameters obtained using the [3]He MRI lung morphometry technique and those measurements found by direct histological analysis.[134,135,139]
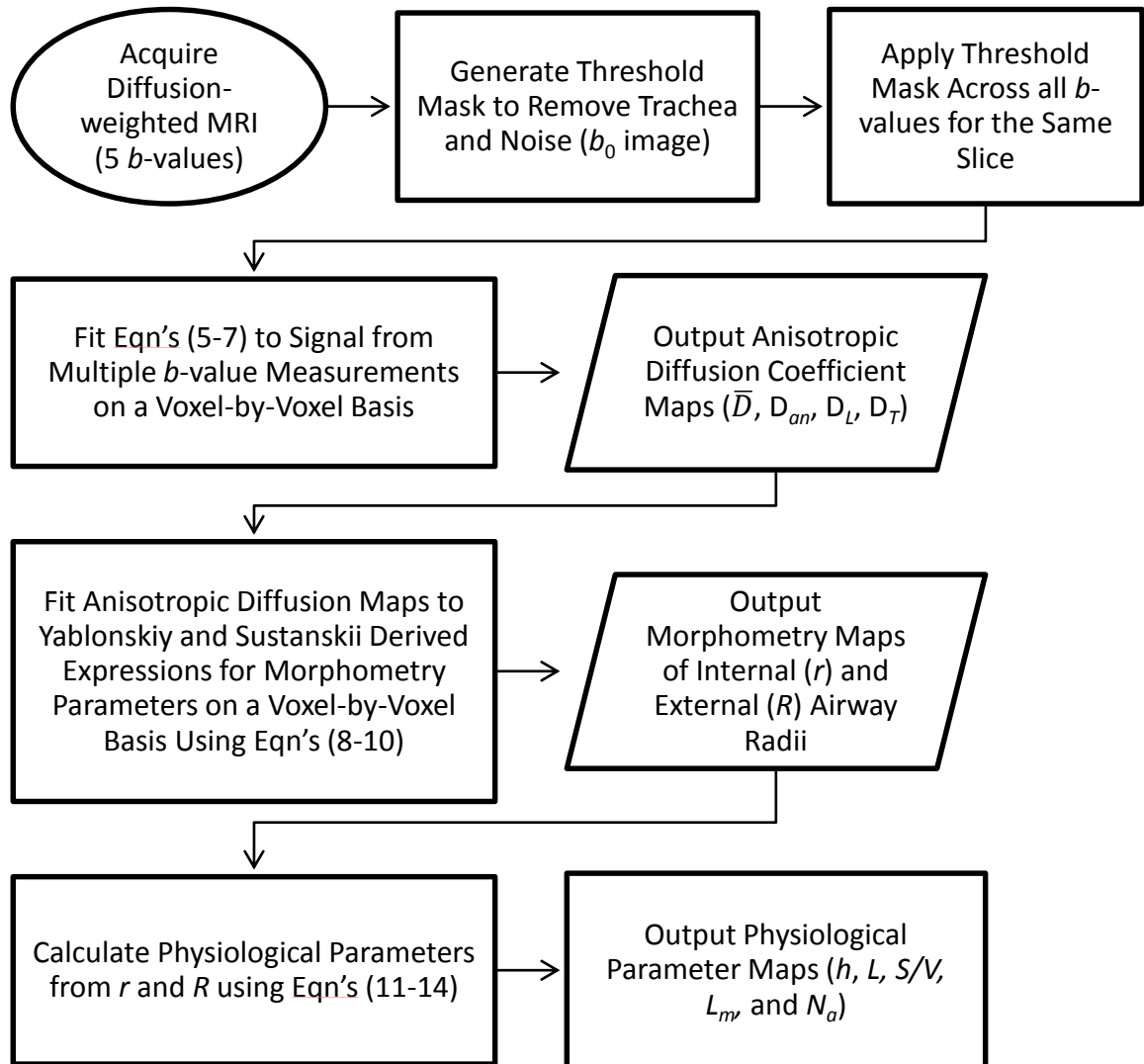
Figure 1-10: Process Diagram for Deriving Physiological Parameters from [3]He Diffusion-weighted MRI. All threshold and fitting procedures were performed using a custom-built IDL 6.4 algorithm. b_0, non-diffusion-weighted image; $\overline{D}$, mean diffusion coefficient; D_{an}, anisotropic diffusion coefficient; D_L, longitudinal diffusion coefficient; D_T, transverse diffusion coefficient; R, external airway radius; r, internal airway radius; h, alveolar sheath; L, alveolar length; S/V, surface area-to-volume ratio; L_m, mean linear intercept; N_a, alveolar density

1.6   Research Hypothesis and Objectives

The hypothesis that we test in this thesis is that older never-smokers will have a significantly increased external airway radius (R) and mean linear intercept (L$_m$), as well

as decreased alveolar sheaths (h) similar to ex-smokers with mild COPD. The primary objective of this thesis was to generate and evaluate ^{3}He MR morphometry measurements in a group of older never-smokers in order to build upon previous hyperpolarized noble gas lung imaging studies of the senile lung. The aim was to develop and apply a non-invasive method for measuring lung morphometry in a group of older-never smokers. By applying the ^{3}He diffusion weighted technique, I acquired estimates of alveolar airspace dimensions and compared those to values calculated for a comparator group of ex-smokers. Previous studies observed that there were mild peripheral ventilation defects in a large number of older never-smokers. However, these defects did not contribute to decreased exercise capacity or dyspnea. The current study aims to take a closer look at alveolar microstructure and assess the structural and functional changes that occur in normal lung aging and determine their relationship with standard pulmonary function measurements.

The last chapter of this thesis will provide an overview and summary of the important findings and conclusions of Chapter 2. The study specific limitations as well as general limitations of the use of hyperpolarized gas MRI will be discussed in addition to the potential alternatives or solutions to these issues. Finally, based on the findings and limitations discussed, a roadmap for future hyperpolarized noble gas MRI studies for use in assessing alveolar microstructure will be addressed.

1.7 References

1   Minino, A. M. Death in the United States, 2011. *NCHS data brief*, 1-8 (2013).

2   Verbeken, E. K. *et al.* The senile lung. Comparison with normal and emphysematous lungs. 2. Functional aspects. *Chest* **101**, 800-809 (1992).

3   Verbeken, E. K. *et al.* The senile lung. Comparison with normal and emphysematous lungs. 1. Structural aspects. *Chest* **101**, 793-799 (1992).

4   Lowery, E. M., Brubaker, A. L., Kuhlmann, E. & Kovacs, E. J. The aging lung. *Clin. Interv. Aging* **8**, 1489-1496, doi:10.2147/cia.s51152 (2013).

5   Janssens, J. P., Pache, J. C. & Nicod, L. P. Physiological changes in respiratory function associated with ageing. *The European respiratory journal* **13**, 197-205 (1999).

6   Enright, P. L., Kronmal, R. A., Manolio, T. A., Schenker, M. B. & Hyatt, R. E. Respiratory muscle strength in the elderly. Correlates and reference values. Cardiovascular Health Study Research Group. *Am J Respir Crit Care Med* **149**, 430-438, doi:10.1164/ajrccm.149.2.8306041 (1994).

7   Dempsey, J. A., Hanson, P. G. & Henderson, K. S. Exercise-induced arterial hypoxaemia in healthy human subjects at sea level. *J. Physiol.* **355**, 161-175 (1984).

8   Harms, C. A., Wetter, T. J., St Croix, C. M., Pegelow, D. F. & Dempsey, J. A. Effects of respiratory muscle work on exercise performance. *Journal of applied physiology (Bethesda, Md. : 1985)* **89**, 131-138 (2000).

9   Sharma, G. & Goodwin, J. Effect of aging on respiratory system physiology and immunology. *Clinical interventions in aging* **1**, 253-260 (2006).

10   Peterson, D. D., Pack, A. I., Silage, D. A. & Fishman, A. P. Effects of aging on ventilatory and occlusion pressure responses to hypoxia and hypercapnia. *Am. Rev. Respir. Dis.* **124**, 387-391 (1981).

11   Effros, R. M. Anatomy, development, and physiology of the lungs. *GI Motility online* (2006).

12   Hsia, C. C., Hyde, D. M., Ochs, M. & Weibel, E. R. Commentaries on viewpoint: use of mean airspace chord length to assess emphysema. To be or not to be-accurate. *Journal of applied physiology (Bethesda, Md. : 1985)* **105**, 1982-1983; author reply 1986-1987 (2008).

13   Mata, J. F. Commentaries on viewpoint: use of mean airspace chord length to assess emphysema. Mean airspace chord length and hyperpolarized gas magnetic-

resonance measurements. *Journal of applied physiology (Bethesda, Md. : 1985)* **105**, 1985; author reply 1986-1987 (2008).

14   Ochs, M. A brief update on lung stereology. *J. Microsc.* **222**, 188-200, doi:10.1111/j.1365-2818.2006.01587.x (2006).

15   Weibel, E. R. & Gomez, D. M. Architecture of the human lung. Use of quantitative methods establishes fundamental relations between size and number of lung structures. *Science* **137**, 577-585 (1962).

16   Sherwood, L. *The Respiratory System. Fundamentals of Physiology*. (Thomson Nelson, 2006).

17   Meyers, A. K. *Respiratory System*. 1st edn, 3-45 (Mosby/Elsevier, 2006).

18   Wanner, A., Salathe, M. & O'Riordan, T. G. Mucociliary clearance in the airways. *Am J Respir Crit Care Med* **154**, 1868-1902, doi:10.1164/ajrccm.154.6.8970383 (1996).

19   Wanner, A. Clinical aspects of mucociliary transport. *Am. Rev. Respir. Dis.* **116**, 73-125 (1977).

20   West, J. B. *Respiratory Physiology: The Essentials*. 8th edn, (Lippincott Williams & Wilkins, 2008).

21   Hansen, J. E., Ampaya, E. P., Bryant, G. H. & Navin, J. J. Branching pattern of airways and air spaces of a single human terminal bronchiole. *J. Appl. Physiol.* **38**, 983-989 (1975).

22   Ochs, M. *et al.* The number of alveoli in the human lung. *Am J Respir Crit Care Med* **169**, 120-124, doi:10.1164/rccm.200308-1107OC (2004).

23   Angus, G. E. & Thurlbeck, W. M. Number of alveoli in the human lung. *J. Appl. Physiol.* **32**, 483-485 (1972).

24   Wasserman, K., Whipp, B. J., Koyl, S. N. & Beaver, W. L. Anaerobic threshold and respiratory gas exchange during exercise. *J. Appl. Physiol.* **35**, 236-243 (1973).

25   Daniels, C. B. & Orgeig, S. Pulmonary surfactant: the key to the evolution of air breathing. *News in physiological sciences : an international journal of physiology produced jointly by the International Union of Physiological Sciences and the American Physiological Society* **18**, 151-157 (2003).

26   Cotes, J. E., Chinn, D. J. & Miller, M. R. *Lung function: physiology, measurement and application in medicine*. (John Wiley & Sons, 2009).

27   Weibel, E. R., Hsia, C. C. & Ochs, M. How much is there really? Why stereology is essential in lung morphometry. *J. Appl. Physiol.* **102**, 459-467 (2007).

28   Bates, J. H. *Lung mechanics: an inverse modeling approach*. (Cambridge University Press, 2009).

29   Ward, M. & Macklem, P. T. The act of breathing and how it fails. *Chest* **97**, 36s-39s (1990).

30   Jones, R. L. & Nzekwu, M.-M. U. The effects of body mass index on lung volumes. *Chest journal* **130**, 827-833 (2006).

31   Marieb, E. N. & Hoehn, K. *Human anatomy & physiology*. (Pearson Education, 2007).

32   Lindh, W., Pooler, M., Tamparo, C., Dahl, B. & Morris, J. *Delmar's comprehensive medical assisting: administrative and clinical competencies*. (Cengage Learning, 2013).

33   Clayton, N. Review Series: Lung function made easy: Assessing lung size. *Chron. Respir. Dis.* **4**, 151-157 (2007).

34   Wilmore, J. H. The use of actual, predicted and constant residual volume in the assessment of the body composition by underwater weighing. *Med. Sci. Sports* **1**, 87-90 (1969).

35   Krumpe, P. E., Knudson, R. J., Parsons, G. & Reiser, K. The aging respiratory system. *Clin. Geriatr. Med.* **1**, 143-175 (1985).

36   Wahba, W. M. Influence of aging on lung function--clinical significance of changes from age twenty. *Anesth. Analg.* **62**, 764-776 (1983).

37   Meyer, K. C. Aging. *Proceedings of the American Thoracic Society* **2**, 433-439, doi:10.1513/pats.200508-081JS (2005).

38   Knudson, R. J., Clark, D. F., Kennedy, T. C. & Knudson, D. E. Effect of aging alone on mechanical properties of the normal adult human lung. *Journal of applied physiology: respiratory, environmental and exercise physiology* **43**, 1054-1062 (1977).

39   Lang, M. R. *et al.* Collagen content of alveolar wall tissue in emphysematous and non-emphysematous lungs. *Thorax* **49**, 319-326 (1994).

40   Sobin, S. S., Fung, Y. C. & Tremer, H. M. Collagen and elastin fibers in human pulmonary alveolar walls. *Journal of applied physiology (Bethesda, Md. : 1985)* **64**, 1659-1675 (1988).

41   Toshima, M., Ohtani, Y. & Ohtani, O. Three-dimensional architecture of elastin and collagen fiber networks in the human and rat lung. *Arch. Histol. Cytol.* **67**, 31-40 (2004).

42   Crapo, R. *The Aging Lung*. (Marcel Dekker Incl, 1993).

43   Tolep, K. & Kelsen, S. G. Effect of aging on respiratory skeletal muscles. *Clin. Chest Med.* **14**, 363-378 (1993).

44   Niewoehner, D. E. & Kleinerman, J. Morphologic basis of pulmonary resistance in the human lung and effects of aging. *J. Appl. Physiol.* **36**, 412-418 (1974).

45   Nagase, T., Fukuchi, Y., Teramoto, S., Matsuse, T. & Orimo, H. Mechanical interdependence in relation to age: effects of lung volume on airway resistance in rats. *Journal of applied physiology (Bethesda, Md. : 1985)* **77**, 1172-1177 (1994).

46   Thurlbeck, W. M. The internal surface area of nonemphysematous lungs. *Am. Rev. Respir. Dis.* **95**, 765-773 (1967).

47   Fletcher, C. & Peto, R. The natural history of chronic airflow obstruction. *Br. Med. J.* **1**, 1645-1648 (1977).

48   Knudson, R. J., Slatin, R., Lebowitz, M. & Burrows, B. The maximal expiratory flow-volume curve. Normal standards, variability, and effects of age. *The American review of respiratory disease* **113**, 587-600 (1976).

49   Schmidt, C., Dickman, M., Gardner, R. & Brough, F. Spirometric standards for healthy elderly men and women. 532 subjects, ages 55 through 94 years. *The American review of respiratory disease* **108**, 933 (1973).

50   Ito, K. & Barnes, P. J. COPD as a disease of accelerated lung aging. *CHEST Journal* **135**, 173-180 (2009).

51   Norris, A. H. Relationship between chest wall and pulmonary compliance and age. *Appl Physiol* **20**, 1211 (1965).

52   Turner, J. M., Mead, J. & Wohl, M. E. Elasticity of human lungs in relation to age. *J. Appl. Physiol.* **25**, 664-671 (1968).

53   Dyer, C. A. & Stockley, R. A. The aging lung. *Rev. Clin. Gerontol.* **16**, 99-111 (2006).

54   Guenard, H. & Marthan, R. Pulmonary gas exchange in elderly subjects. *Eur. Respir. J.* **9**, 2573-2577 (1996).

55   Gibson, G. J. *Clinical Tests of Respiratory Function 3rd Edition*. (CRC Press, 2008).

56   Butler 2nd, C. & Kleinerman, J. Capillary density: alveolar diameter, a morphometric approach to ventilation and perfusion. *The American review of respiratory disease* **102**, 886 (1970).

57   Gossner, J. & Nau, R. Geriatric chest imaging: when and how to image the elderly lung, age-related changes, and common pathologies. *Radiology research and practice* **2013**, 584793, doi:10.1155/2013/584793 (2013).

58   Daftari Besheli, L., Aran, S., Shaqdan, K., Kay, J. & Abujudeh, H. Current status of nephrogenic systemic fibrosis. *Clin. Radiol.* **69**, 661-668, doi:10.1016/j.crad.2014.01.003 (2014).

59   Copley, S. J. *et al.* Lung morphology in the elderly: comparative CT study of subjects over 75 years old versus those under 55 years old. *Radiology* **251**, 566-573, doi:10.1148/radiol.2512081242 (2009).

60   Lee, K. W. *et al.* Correlation of aging and smoking with air trapping at thin-section CT of the lung in asymptomatic subjects. *Radiology* **214**, 831-836, doi:10.1148/radiology.214.3.r00mr05831 (2000).

61   Sheikh, K. *et al.* Pulmonary ventilation defects in older never-smokers. *Journal of applied physiology (Bethesda, Md. : 1985)* **117**, 297-306, doi:10.1152/japplphysiol.00046.2014 (2014).

62   Mayer, E., Blazsik, C. & Rappaport, I. Emphysema and the Lungs of the Aged: A Clinical StudyPreliminary Report. *Chest* **34**, 247-256 (1958).

63   Gillooly, M. & Lamb, D. Airspace size in lungs of lifelong non-smokers: effect of age and sex. *Thorax* **48**, 39-43 (1993).

64   Young Jr, R. C., Borden, D. L. & Rachal, R. E. Aging of the lung: pulmonary disease in the elderly. *Age* **10**, 138-145 (1987).

65   Kronenberg, R. S. & Drage, C. W. Attenuation of the ventilatory and heart rate responses to hypoxia and hypercapnia with aging in normal men. *J. Clin. Invest.* **52**, 1812 (1973).

66   Laennec, R. T. H. & Forbes, J. *A Treatise on the Diseases of the Chest, and on Mediate Auscultation*. (Samuel S. and William Wood, 1834).

67   Hogg, J. C. Pathophysiology of airflow limitation in chronic obstructive pulmonary disease. *Lancet* **364**, 709-721, doi:10.1016/s0140-6736(04)16900-6 (2004).

68   Verschakelen, J., De Wever, W. & Matamoros, A. Computed Tomography of the Lung: A Pattern Approach. *J. Nucl. Med.* **49**, 164-164 (2008).

69   Kim, W. D. *et al.* Centrilobular and panlobular emphysema in smokers. Two distinct morphologic and functional entities. *Am. Rev. Respir. Dis.* **144**, 1385-1390, doi:10.1164/ajrccm/144.6.1385 (1991).

70   Anderson, A. E., Jr. & Foraker, A. G. Centrilobular emphysema and panlobular emphysema: two different diseases. *Thorax* **28**, 547-550 (1973).

71   Coxson, H. O. *et al.* New and current clinical imaging techniques to study chronic obstructive pulmonary disease. *Am J Respir Crit Care Med* **180**, 588-597, doi:10.1164/rccm.200901-0159PP (2009).

72   Coxson, H. O. & Rogers, R. M. Quantitative computed tomography of chronic obstructive pulmonary disease. *Academic radiology* **12**, 1457-1463, doi:10.1016/j.acra.2005.08.013 (2005).

73   Ochs, M. & Muhlfeld, C. Quantitative microscopy of the lung: a problem-based approach. Part 1: basic principles of lung stereology. *Am. J. Physiol. Lung Cell Mol. Physiol.* **305**, L15-22, doi:10.1152/ajplung.00429.2012 (2013).

74   Baddeley, A. & Jensen, E. B. V. *Stereology for statisticians*. (CRC Press, 2004).

75   Miles, R. & Davy, P. Precise and general conditions for the validity of a comprehensive set of stereological fundamental formulae. *J. Microsc.* **107**, 211-226 (1976).

76   Mayhew, T. M., Mühlfeld, C., Vanhecke, D. & Ochs, M. A review of recent methods for efficiently quantifying immunogold and other nanoparticles using TEM sections through cells, tissues and organs. *Annals of Anatomy-Anatomischer Anzeiger* **191**, 153-170 (2009).

77   Vasilescu, D. M. *et al.* Assessment of morphometry of pulmonary acini in mouse lungs by nondestructive imaging using multiscale microcomputed tomography. *Proceedings of the National Academy of Sciences* **109**, 17105-17110 (2012).

78   Kellner, M. *et al.* Imaging of the mouse lung with scanning laser optical tomography (SLOT). *Journal of applied physiology (Bethesda, Md. : 1985)* **113**, 975-983, doi:10.1152/japplphysiol.00026.2012 (2012).

79   Hsia, C. C., Hyde, D. M., Ochs, M. & Weibel, E. R. An official research policy statement of the American Thoracic Society/European Respiratory Society: standards for quantitative assessment of lung structure. *Am. J. Respir. Crit. Care Med.* **181**, 394-418 (2010).

80   Fehrenbach, H. Animal models of pulmonary emphysema: a stereologist's perspective. *European Respiratory Review* **15**, 136-147 (2006).

81   Knudsen, L., Weibel, E. R., Gundersen, H. J. G., Weinstein, F. V. & Ochs, M. Assessment of air space size characteristics by intercept (chord) measurement: an

accurate and efficient stereological approach. *J. Appl. Physiol.* **108**, 412-421 (2010).

82   Mühlfeld, C. & Ochs, M. Quantitative microscopy of the lung: a problem-based approach. Part 2: stereological parameters and study designs in various diseases of the respiratory tract. *American Journal of Physiology-Lung Cellular and Molecular Physiology* **305**, L205-L221 (2013).

83   Joarder, R. & Crundwell, N. *Chest X-ray in clinical practice.* (Springer, 2009).

84   Buzug, T. M. *Computed tomography: from photon statistics to modern cone-beam CT.* (Springer, 2008).

85   Kim, W. J. *et al.* CT metrics of airway disease and emphysema in severe COPD. *Chest* **136**, 396-404, doi:10.1378/chest.08-2858 (2009).

86   Nakano, Y. *et al.* Computed tomographic measurements of airway dimensions and emphysema in smokers. Correlation with lung function. *Am J Respir Crit Care Med* **162**, 1102-1108, doi:10.1164/ajrccm.162.3.9907120 (2000).

87   Nakano, Y. *et al.* The prediction of small airway dimensions using computed tomography. *Am. J. Respir. Crit. Care Med.* **171**, 142-146 (2005).

88   Bankier, A. A., De Maertelaer, V., Keyzer, C. & Gevenois, P. A. Pulmonary Emphysema: Subjective Visual Grading versus Objective Quantification with Macroscopic Morphometry and Thin-Section CT Densitometry 1. *Radiology* **211**, 851-858 (1999).

89   Bankier, A. A., Madani, A. & Gevenois, P. A. CT quantification of pulmonary emphysema: assessment of lung structure and function. *Critical reviews in computed tomography* **43**, 397-415 (2002).

90   Salomé, M. *et al.* A synchrotron radiation microtomography system for the analysis of trabecular bone samples. *Med. Phys.* **26**, 2194-2204 (1999).

91   Holdsworth, D. W. & Thornton, M. M. Micro-CT in small animal and specimen imaging. *Trends Biotechnol.* **20**, S34-S39 (2002).

92   Vasilescu, D. M. *et al.* Stereological assessment of mouse lung parenchyma via nondestructive, multiscale micro-CT imaging validated by light microscopic histology. *J. Appl. Physiol.* **114**, 716-724 (2013).

93   Tsuda, A. *et al.* Finite element 3D reconstruction of the pulmonary acinus imaged by synchrotron X-ray tomography. *Journal of applied physiology (Bethesda, Md. : 1985)* **105**, 964-976, doi:10.1152/japplphysiol.90546.2008 (2008).

94   Schittny, J. C., Mund, S. I. & Stampanoni, M. Evidence and structural mechanism for late lung alveolarization. *Am. J. Physiol. Lung Cell Mol. Physiol.* **294**, L246-254, doi:10.1152/ajplung.00296.2007 (2008).

95   Parameswaran, H. *et al.* Three-dimensional measurement of alveolar airspace volumes in normal and emphysematous lungs using micro-CT. *J. Appl. Physiol.* **107**, 583-592 (2009).

96   Litzlbauer, H. D. *et al.* Three-dimensional imaging and morphometric analysis of alveolar tissue from microfocal X-ray-computed tomography. *American Journal of Physiology-Lung Cellular and Molecular Physiology* **291**, L535-L545 (2006).

97   Watz, H., Breithecker, A., Rau, W. S. & Kriete, A. Micro-CT of the human lung: imaging of alveoli and virtual endoscopy of an alveolar duct in a normal lung and in a lung with centrilobular emphysema--initial observations. *Radiology* **236**, 1053-1058, doi:10.1148/radiol.2363041142 (2005).

98   Litzlbauer, H. D. *et al.* Synchrotron-based micro-CT imaging of the human lung acinus. *Anat Rec (Hoboken)* **293**, 1607-1614, doi:10.1002/ar.21161 (2010).

99   McDonough, J. E. *et al.* Small-airway obstruction and emphysema in chronic obstructive pulmonary disease. *N. Engl. J. Med.* **365**, 1567-1575 (2011).

100   Kauczor, H. U. & Kreitner, K. F. MRI of the pulmonary parenchyma. *European radiology* **9**, 1755-1764, doi:10.1007/s003300050919 (1999).

101   Puderbach, M. *et al.* MR imaging of the chest: a practical approach at 1.5T. *European journal of radiology* **64**, 345-355, doi:10.1016/j.ejrad.2007.08.009 (2007).

102   Kauczor, H. U., Ley-Zaporozhan, J. & Ley, S. Imaging of pulmonary pathologies: focus on magnetic resonance imaging. *Proceedings of the American Thoracic Society* **6**, 458-463, doi:10.1513/pats.200901-002AW (2009).

103   Mayo, J. R., MacKay, A. & Muller, N. L. MR imaging of the lungs: value of short TE spin-echo pulse sequences. *AJR Am. J. Roentgenol.* **159**, 951-956, doi:10.2214/ajr.159.5.1414805 (1992).

104   Togao, O., Tsuji, R., Ohno, Y., Dimitrov, I. & Takahashi, M. Ultrashort echo time (UTE) MRI of the lung: assessment of tissue density in the lung parenchyma. *Magn. Reson. Med.* **64**, 1491-1498, doi:10.1002/mrm.22521 (2010).

105   Failo, R. *et al.* Lung morphology assessment using MRI: a robust ultra-short TR/TE 2D steady state free precession sequence used in cystic fibrosis patients. *Magn. Reson. Med.* **61**, 299-306, doi:10.1002/mrm.21841 (2009).

106   Albert, M. S. *et al.* Biological magnetic resonance imaging using laser-polarized 129Xe. *Nature* **370**, 199-201, doi:10.1038/370199a0 (1994).

107   Kirby, M. *et al.* Chronic obstructive pulmonary disease: longitudinal hyperpolarized (3)He MR imaging. *Radiology* **256**, 280-289, doi:10.1148/radiol.10091937 (2010).

108   Marshall, H. *et al.* Direct visualisation of collateral ventilation in COPD with hyperpolarised gas MRI. *Thorax* **67**, 613-617, doi:10.1136/thoraxjnl-2011-200864 (2012).

109   Mathew, L. *et al.* Hyperpolarized (3)He magnetic resonance imaging: preliminary evaluation of phenotyping potential in chronic obstructive pulmonary disease. *European journal of radiology* **79**, 140-146, doi:10.1016/j.ejrad.2009.10.028 (2011).

110   de Lange, E. E. *et al.* Evaluation of asthma with hyperpolarized helium-3 MRI: correlation with clinical severity and spirometry. *Chest* **130**, 1055-1062, doi:10.1378/chest.130.4.1055 (2006).

111   Fain, S. B. *et al.* Evaluation of structure-function relationships in asthma using multidetector CT and hyperpolarized He-3 MRI. *Academic radiology* **15**, 753-762, doi:10.1016/j.acra.2007.10.019 (2008).

112   Tustison, N. J. *et al.* Feature analysis of hyperpolarized helium-3 pulmonary MRI: a study of asthmatics versus nonasthmatics. *Magn. Reson. Med.* **63**, 1448-1455, doi:10.1002/mrm.22390 (2010).

113   Kirby, M. *et al.* Quantitative evaluation of hyperpolarized helium-3 magnetic resonance imaging of lung function variability in cystic fibrosis. *Academic radiology* **18**, 1006-1013, doi:10.1016/j.acra.2011.03.005 (2011).

114   Mentore, K. *et al.* Hyperpolarized HHe 3 MRI of the lung in cystic fibrosis: assessment at baseline and after bronchodilator and airway clearance treatment. *Academic radiology* **12**, 1423-1429, doi:10.1016/j.acra.2005.07.008 (2005).

115   Paulin, G. A. *et al.* Differences in hyperpolarized He ventilation imaging after 4 years in adults with cystic fibrosis. *Journal of magnetic resonance imaging : JMRI*, doi:10.1002/jmri.24744 (2014).

116   Mathew, L. *et al.* Hyperpolarized (3)He magnetic resonance imaging: comparison with four-dimensional x-ray computed tomography imaging in lung cancer. *Academic radiology* **19**, 1546-1553, doi:10.1016/j.acra.2012.08.007 (2012).

117   Kirby, M. *et al.* Hyperpolarized 3He magnetic resonance functional imaging semiautomated segmentation. *Academic radiology* **19**, 141-152, doi:10.1016/j.acra.2011.10.007 (2012).

118   Parraga, G. *et al.* Hyperpolarized 3He ventilation defects and apparent diffusion coefficients in chronic obstructive pulmonary disease: preliminary results at 3.0

Tesla. *Investigative radiology* **42**, 384-391, doi:10.1097/01.rli.0000262571.81771.66 (2007).

119   Salerno, M., Altes, T. A., Brookeman, J. R., de Lange, E. E. & Mugler, J. P., 3rd. Rapid hyperpolarized 3He diffusion MRI of healthy and emphysematous human lungs using an optimized interleaved-spiral pulse sequence. *Journal of magnetic resonance imaging : JMRI* **17**, 581-588, doi:10.1002/jmri.10303 (2003).

120   Mugler, J. P., 3rd *et al.* Helium-3 diffusion MR imaging of the human lung over multiple time scales. *Academic radiology* **15**, 693-701, doi:10.1016/j.acra.2007.10.009 (2008).

121   Saam, B. T. *et al.* MR imaging of diffusion of (3)He gas in healthy and diseased lungs. *Magn. Reson. Med.* **44**, 174-179 (2000).

122   Stejskal, E. Use of Spin Echoes in a Pulsed Magnetic-Field Gradient to Study Anisotropic, Restricted Diffusion and Flow. *The Journal of Chemical Physics* **43**, 3597-3603 (1965).

123   Basser, P. J., Mattiello, J. & LeBihan, D. MR diffusion tensor spectroscopy and imaging. *Biophys. J.* **66**, 259-267, doi:10.1016/S0006-3495(94)80775-1 (1994).

124   Yablonskiy, D. A. *et al.* Quantitative in vivo assessment of lung microstructure at the alveolar level with hyperpolarized 3He diffusion MRI. *Proc. Natl. Acad. Sci. U. S. A.* **99**, 3111-3116, doi:10.1073/pnas.052594699 (2002).

125   Fain, S. B. *et al.* Detection of Age-Dependent Changes in Healthy Adult Lungs With Diffusion-Weighted 3He MRI. *Acad. Radiol.* **12**, 1385-1393 (2005).

126   Saam, B. T. *et al.* MR imaging of diffusion of 3He gas in healthy and diseased lungs. *Magn. Reson. Med.* **44**, 174-179 (2000).

127   Parraga, G. *et al.* Hyperpolarized 3He ventilation defects and apparent diffusion coefficients in chronic obstructive pulmonary disease: preliminary results at 3.0 Tesla. *Invest. Radiol.* **42**, 384-391 (2007).

128   Morbach, A. E. *et al.* Diffusion-weighted MRI of the lung with hyperpolarized helium-3: A study of reproducibility. *J. Magn. Reson. Imaging* **21**, 765-774 (2005).

129   Diaz, S. *et al.* Hyperpolarized 3He apparent diffusion coefficient MRI of the lung: reproducibility and volume dependency in healthy volunteers and patients with emphysema. *J. Magn. Reson. Imaging* **27**, 763-770 (2008).

130   Diaz, S. *et al.* Validity of apparent diffusion coefficient hyperpolarized 3He-MRI using MSCT and pulmonary function tests as references. *Eur. J. Radiol.* **71**, 257-263 (2009).

131   Fain, S. B. *et al.* Early Emphysematous Changes in Asymptomatic Smokers: Detection with 3He MR Imaging 1. *Radiology* **239**, 875-883 (2006).

132   Woods, J. C. *et al.* Hyperpolarized 3He diffusion MRI and histology in pulmonary emphysema. *Magn. Reson. Med.* **56**, 1293-1300 (2006).

133   Swift, A. J. *et al.* Emphysematous changes and normal variation in smokers and COPD patients using diffusion< sup> 3</sup> He MRI. *Eur. J. Radiol.* **54**, 352-358 (2005).

134   Yablonskiy, D. A. *et al.* Quantitative in vivo assessment of lung microstructure at the alveolar level with hyperpolarized 3He diffusion MRI. *Proceedings of the National Academy of Sciences* **99**, 3111-3116 (2002).

135   Yablonskiy, D. A. *et al.* Quantification of lung microstructure with hyperpolarized 3He diffusion MRI. *Journal of applied physiology (Bethesda, Md. : 1985)* **107**, 1258-1265, doi:10.1152/japplphysiol.00386.2009 (2009).

136   Quirk, J. D. *et al.* In vivo detection of acinar microstructural changes in early emphysema with 3He lung morphometry. *Radiology* **260**, 866-874 (2011).

137   Ouriadov, A. *et al.* Lung morphometry using hyperpolarized (129) Xe apparent diffusion coefficient anisotropy in chronic obstructive pulmonary disease. *Magn. Reson. Med.* **70**, 1699-1706, doi:10.1002/mrm.24595 (2013).

138   Quirk, J. D., Chang, Y. V. & Yablonskiy, D. A. In vivo lung morphometry with hyperpolarized He diffusion MRI: Reproducibility and the role of diffusion-sensitizing gradient direction. *Magn. Reson. Med.*, doi:10.1002/mrm.25241 (2014).

139   Sukstanskii, A. L., Quirk, J. D. & Yablonskiy, D. A. Probing lung microstructure with hyperpolarized 3He gradient echo MRI. *NMR Biomed.* **27**, 1451-1460, doi:10.1002/nbm.3150 (2014).

140   Yablonskiy, D. A., Sukstanskii, A. L., Quirk, J. D., Woods, J. C. & Conradi, M. S. Probing lung microstructure with hyperpolarized noble gas diffusion MRI: theoretical models and experimental results. *Magn. Reson. Med.*, doi:10.1002/mrm.24729 (2013).

141   Weibel, E. R., Crystal, R. G., West, J. B., Barnes, P. J. & Cherniack, N. S. *The lung: scientific foundations*. (Raven Press, 1991).

142   Haefeli-Bleuer, B. & Weibel, E. R. Morphometry of the human pulmonary acinus. *Anat. Rec.* **220**, 401-414, doi:10.1002/ar.1092200410 (1988).

143   Phalen, R. & Oldham, M. Tracheobronchial airway structure as revealed by casting techniques. *The American review of respiratory disease* **128**, S1-4 (1983).

144   Bastacky, J., Hayes, T. & Von Schmidt, B. Lung structure as revealed by microdissection. Positional morphology of human lung. *The American review of respiratory disease* **128**, S7-13 (1983).

145   Plopper, C., Mariassy, A. & Lollini, L. Structure as revealed by airway dissection. A comparison of mammalian lungs. *The American review of respiratory disease* **128**, S4-7 (1983).

146   Callaghan, P. T. *Principles of nuclear magnetic resonance microscopy*. Vol. 3 (Clarendon Press Oxford, 1991).

147   Sukstanskii, A. L. & Yablonskiy, D. A. In vivo lung morphometry with hyperpolarized 3He diffusion MRI: theoretical background. *J. Magn. Reson.* **190**, 200-210, doi:10.1016/j.jmr.2007.10.015 (2008).

148   Sukstanskii, A. L., Conradi, M. S. & Yablonskiy, D. A. (3)He lung morphometry technique: accuracy analysis and pulse sequence optimization. *J. Magn. Reson.* **207**, 234-241, doi:10.1016/j.jmr.2010.09.005 (2010).

2 CHAPTER 2: MULTIPLE B VALUE [3]HE MRI OF OLDER NEVER SMOKERS

To better understand the senile lung and the morphometric changes that occur with age, here we evaluated a group of older never-smokers as well as a small group of ex-smokers using hyperpolarized [3]He diffusion weighted MRI to provide quantitative measurements of lung morphometry.

2.1 Introduction

Senile emphysema is characterized by distal airway enlargement without obvious fibrosis or alveolar wall destruction.[1] Other structural components of senile lung include the loss of elastic fibers, thickening of alveolar walls[1], and diminished pulmonary elastic recoil.[2-4] In concert with the pathological changes that accompany aging, increased residual volume (RV), functional residual capacity (FRC) [5], and decreased diffusing capacity of carbon monoxide (DL_{CO}) [5], forced expiratory volume in 1 sec (FEV_1), and forced vital capacity (FVC) [6] are also observed.

Senile emphysema is often considered to be a misnomer, as subjects do not express the same clinical symptoms of emphysema, and this condition is more appropriately referred to as the senile lung. [7] Specifically, emphysema as found in chronic obstructive pulmonary disease (COPD) is differentiated structurally from senile lung by the deformation of alveoli as a result of fibrosis and tissue destruction, resulting in reduced surface area for gas exchange.[8] Importantly, subjects with senile lung appear to have sufficient lung function for their normal day-to-day activities.[9] These changes do however increase the risk of breathlessness and respiratory failure in the elderly when compromised, and further complicate health when combined with cardiac impairment or respiratory infection.[10-12] Specifically, these age-dependent structural and functional changes can reduce sensitivity of the respiratory centres in the presence of hypoxia or hypercapnia, resulting in a diminished ventilatory response in cases of heart failure or aggravated airways obstruction.[5,10,13]

Although the changes associated with senile emphysema are histologically different from COPD- related emphysema, they result in similar changes in lung compliance and function. A consequence of the reduction in supporting tissues around the airways is a tendency for the smaller airways to collapse. As a result, premature closure of these airways (<2mm) becomes common during normal tidal breathing.

Hyperpolarized inhaled noble gas magnetic resonance imaging (MRI) provides non-invasive measurements of lung function and structure [14-19] showing those regions of the lung that participate in ventilation and those that do not.[19,20] In addition, the MRI apparent diffusion coefficient (ADC) for an inhaled gas is sensitive to changes in the lung microstructure and airspace size correlating well with age [17], spirometry [21], DL_{CO} [22], and x-ray computed tomography (CT) measurements of emphysema [23]. Previous studies have shown a close agreement between alveolar parameters obtained using the ^{3}He MRI lung morphometry technique and those found by direct histological analysis.[24] Many of these studies have shown a close link between elevated alveolar sheath dimensions and mean linear intercept with pulmonary function measurements, in mild to severe cases of COPD.[24-26] As such, we hypothesize that older never-smokers will have a significantly increased external airway radius (R) and mean linear intercept (L_m), as well as a decreased alveolar sheath (h) as compared to younger never-smokers, that is similar to ex-smokers with mild-to-moderate COPD.

2.2   Methods

2.2.1   Study Subjects and Design

Participants provided written informed consent to the study protocol approved by the local research ethics board and Health Canada. An older never-smoker group of subjects (60-90 years of age) with ≤ 0.5 pack year smoking history and without acute or chronic respiratory disease, as well as a comparator ex-smoker group, were evaluated using spirometry, plethysmography, hyperpolarized ^{3}He MRI and CT during a single visit.

2.2.2   Pulmonary Function Measures

Spirometry was performed to acquire the forced expiratory volume in one second (FEV_1), forced vital capacity (FVC), and FEV_1/FVC according to American Thoracic Society (ATS) guidelines (MedGraphics Corporation, St. Paul, Minnesota, USA).[27] Body plethysmography was performed for the measurement of lung volumes, and DL_{CO} was measured using the gas analyzer (MedGraphics, St. Paul, MN).

2.2.3   Image Acquisition Parameters

MRI was performed on a whole body 3T MRI system (MR750 Discovery, GEHC, Milwaukee, WI) with broadband imaging capability. All ^{3}He MRI employed a whole body gradient set with maximum gradient amplitude of 4.8 G/cm and a single-channel, rigid elliptical transmit/receive chest coil (RAPID Biomedical GmbH, Wuerzburg, Germany). The basis frequency of the coil was 97.3 MHz and excitation power was 2 kW using an AMT 3T90 RF power amplifier (GEHC). Subjects were positioned supine in the scanner and for both ^{1}H and ^{3}He MRI, subjects were instructed by a pulmonary function technologist to inhale a gas mixture from functional residual capacity (FRC), and image acquisition was performed under breath-hold conditions. Proton MRI and ^{3}He static ventilation images were acquired as previously described.[18] The data for in vivo lung morphometry were acquired using a multi-slice 2D gradient echo diffusion weighted sequence with a matrix size of 128x80, for each of seven 30mm coronal slices (flip angle $\theta = 4°$, TE = 1.2 ms, TR=4.7 ms, b= 0, 1.6, 3.2, 4.8, 6.4 s/cm^2); the diffusion-sensitization gradient pulse ramp up/down time = 500 μs with a diffusion time = 1460 μs and no gap between lobes. All five interleaved sets of images were acquired during a single breath-hold.

Thoracic CT was acquired on a 64-slice Lightspeed VCT scanner (GEHC) (64 $\times$ 0.625 mm, 120 kVp, 100 effective mA, tube rotation time of 500 msec, and a pitch of 1.0). A single spiral acquisition of the entire lung was acquired from the apex to the base with subjects in the supine position and in breath-hold after inhalation of a 1.0 L ^{4}He/N_2 mixture from FRC. Images were reconstructed using a slice thickness of 1.25 mm with a standard convolution kernel. The total effective dose for an average adult was 1.8 mSv.

2.2.4   Image Analysis

Ventilation defect percent (VDP) measurements were generated by one observer using semi-automated segmentation software as previously described.[28] ^{3}He MRI ADC analysis was performed using MATLAB R2013b (MathWorks, Natick, MA). To ensure that ADC was generated for voxels corresponding to ventilated lung regions, a k-means clustering algorithm, developed previously for ^{3}He MRI segmentation[28], was applied to the nondiffusion-weighted images (b= 0 s/cm^2) to obtain a binary mask for each slice. The resulting binary masks were then applied to the corresponding diffusion-weighted images (b= 1.6 s/cm^2), and the ADC maps were generated on a voxel-by-voxel basis. The relative area of the CT density histogram with attenuation values less than −950 Hounsfield units (RA$_{950}$) was determined using Pulmonary Workstation 2.0 (VIDA Diagnostics Inc., Coralville, IA). A CT density threshold for emphysema of RA$_{950}$ greater than 6.8% was used based on a previous study that reported this value as the upper 95% limit of predicted normal values.[29]

2.2.5   Lung Morphometry Calculation

As previously described[30], external (R) and internal (r) airway radius parametric maps were computed from diffusion-weighted data on a pixel-by-pixel basis using a custom-built IDL 6.4 algorithm which searched for the global minimum to determine longitudinal (D_L) and transverse (D_T) diffusion coefficients from mean ($\overline{D}$) and anisotropic (D_{an}) diffusion coefficients. To extract diffusion coefficients, the conditions $b_{max}D_{an}$>1 and $b_{max}D_T > 1$ must be met, where b_{max} is the maximum b-value in the experiment. These constraints define the minimal gradient strength necessary for extracting the diffusion coefficients D$_L$ and D$_T$ from the multiple b-value MR experiments, while maintaining a constant diffusion time for each b-value acquisition.[31] The free diffusion coefficient of ^{3}He gas in lung airspaces (D$_0$) was determined to be concentration-independent and assumed to be 0.84 cm^2/s. All morphometry modelling was performed within the physiological range of r/R>0.4. Estimates of alveolar density (N_a), surface area-to-volume ratio (S/V) and mean linear intercept (L_m) were also generated as previously described.[24]

2.2.6 Statistical Analysis

Measurement comparisons were performed using a Wilcoxon matched-pairs two-tailed t-test using IBM SPSS Statistics 20.00 (SPSS, Chicago, IL). Multiple comparisons were evaluated using the Kruskal-Wallis test with Dunn's correction while relationships between morphometry and spirometry measurements were evaluated using linear regression (R^2) analysis (least squares method) performed using GraphPad Prism 4.01 (GraphPad Software, La Jolla, CA; 2004); best fit lines and the corresponding 95% confidence intervals were determined. Results were considered statistically significant when the probability of making a Type I error was less than 5% ($p < 0.05$).

2.3 Results

2.3.1 Subject Demographics and Pulmonary Function Measurements

Forty-two older never-smokers (73±6yrs, 19 males) and a comparator group consisting of 25 age-matched ex-smokers (71±10yrs, 18 males) were enrolled in the study. Table 2-1 shows subject demographics as well as pulmonary function test results for all subjects. Significant differences were observed between the two groups for FEV_1 (p=.001), FEV_1/FVC (p<.001), RV (p=.009) and DL_{CO} (p<.001). There were no significant differences (p>.05) in Age, BMI, FVC, TLC and RV/TLC between the two groups.

Table 2-1: Subject Demographics

Parameter (±SD)	Older Never-Smokers (n=42)	Ex-Smokers (n=25)	Significance of difference (p-value)
Sex (male)	19	18	-
Age (yrs)	73 (6)	71 (10)	ns
BMI (kg $\cdot m^{-2}$)	27 (4)	28 (5)	ns
FEV $_{1\%pred}$	107 (17)	88 (28)	**.001**
FVC $_{\%pred}$	103 (15)	97 (21)	ns
FEV_1/FVC %	77 (6)	66 (14)	**<.001**
RV %$_{pred}$	98 (22)	118 (39)	**.009**
TLC %$_{pred}$	101 (13)	100 (27)	ns
RV/TLC %$_{pred}$	97 (16)	108 (35)	ns
DL_{CO} %$_{pred}$	90 (16)*	67 (26)	**<.001**

SD, standard deviation; BMI, body mass index; FEV_1, forced expiratory volume in 1 second; %pred, percent predicted; FVC, forced vital capacity; RV, residual volume; TLC, total lung capacity; DL_{CO}, diffusing capacity of the lung for carbon monoxide. *n=39

2.3.2   Imaging Measurements

Figure 2-1 shows the central coronal ^{3}He static ventilation and morphometry maps for a representative older never-smoker and an ex-smoker. Difference in shape of static ventilation images as compared to morphometry maps can be explained by differences in slice thickness between static ventilation and diffusion-weighted images. Table 2-2 shows ^{3}He MR measurements as well as the CT surrogate measure of emphysema (RA$_{950}$) for all subjects. All ^{3}He ventilation (VDP), diffusion (ADC, D_L, and D_L) and morphometry (R, r, h, L_m, N_a, S/V) measurements, as well as CT-derived RA$_{950}$ were significantly different between the two groups. In addition, when compared to literature reported values for a small group of younger never-smokers, using both CT and the ^{3}He morphometry technique, older never-smokers appeared to have a greater acinar duct radius (R= 330 and 300μm respectively) and mean linear intercept (h=240 and 210μm), although sample size was not large enough to show significance.[24,32]
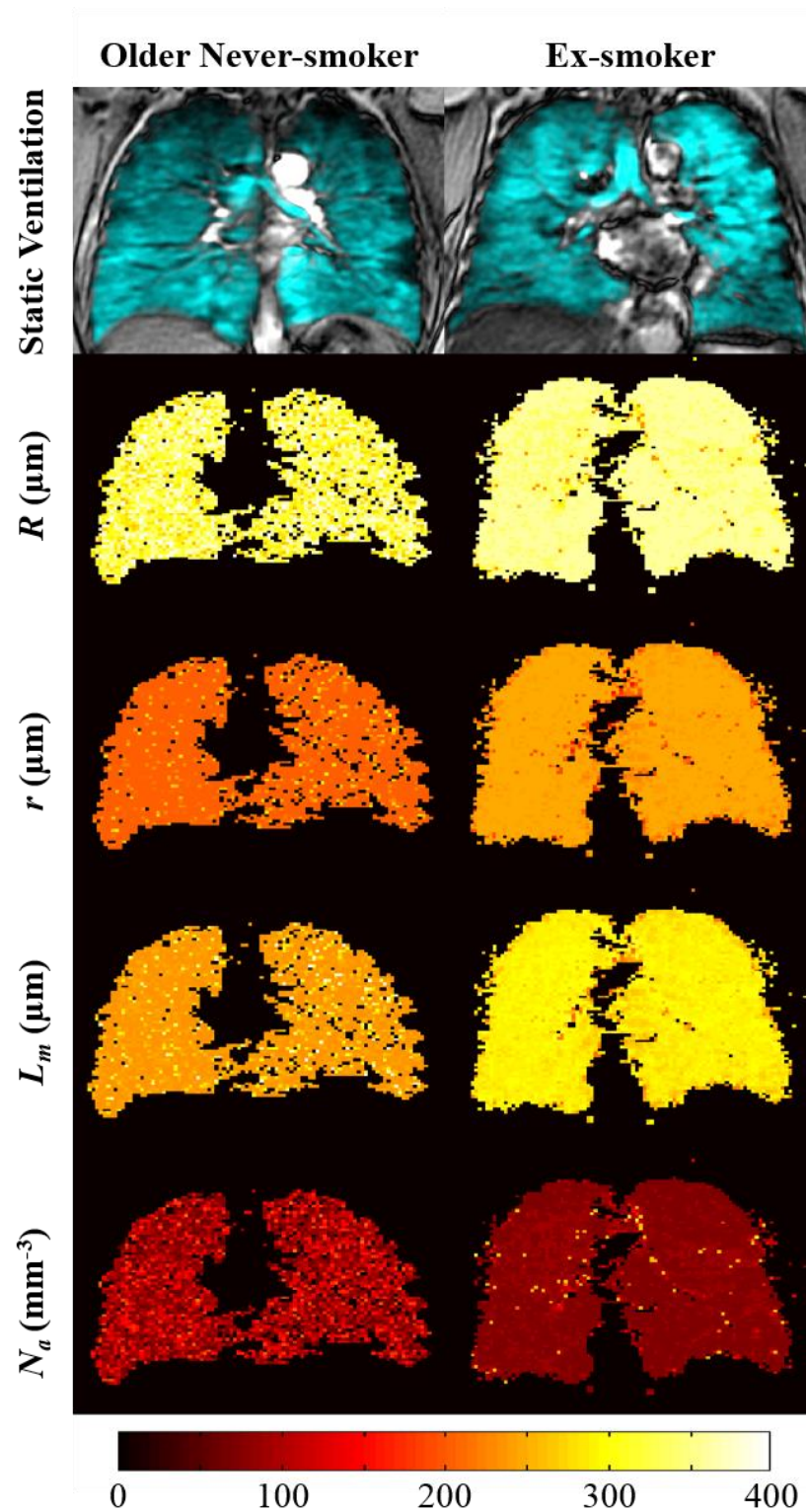
Figure 2-1: ³He Centre Slice Static Ventilation and Morphometry Maps. Hyperpolarized ³He static ventilation and morphometry maps for an older never-smoker (f, 77yr) and an ex-smoker (f, 67yr). *R*, external airway radii; *r*, internal airway radii; *h*, alveolar sheath; L_m, mean linear intercept; N_a, alveolar density.

Table 2-2: ³He MRI Ventilation, ADC, Lung Morphometry and CT measurements

Parameter (±SD)	Older Never-Smokers (n=42)	Ex-Smokers (n=25)	Significance of difference (p-value)
VDP (%)	3 (2)	15 (11)	**<.001**
ADC	0.29 (0.03)	0.34 (0.06)	**<.001**
D_L	0.81 (0.17)*	0.59 (0.19)	**<.001**
D_T	0.32 (0.07)*	0.46 (0.08)	**<.001**
R (µm)	327 (4)*	336 (14)	**<.001**
r (µm)	205 (3)*	227 (12)	**<.001**
h (µm)	122 (4)*	109 (16)	**<.001**
L_m (µm)	244 (4)*	272 (14)	**<.001**
N_a (mm⁻³)	103 (3)*	95 (14)	**.003**
S/V (cm⁻¹)	163 (3)*	147 (7)	**<.001**
RA$_{950}$ (%)	0.73 (0.75)	7.4 (9.1)	**<.001**

VDP, ventilation defect percent; ADC, apparent diffusion coefficient; D_L, longitudinal diffusion coefficient; D_T, transverse diffusion coefficient; R, external airway radius; r, internal airway radius; h, alveolar sheath; L_m, mean linear intercept; N_a, alveolar density; S/V, surface area-to-volume ratio; RA$_{950}$, relative area under -950 Hounsfield units. *n=40

As shown in Figure 2-2, for older never-smokers (NS), external airway radius (R) was significantly smaller (p<.05), alveolar sheath (h) was significantly greater (p<.05), and alveolar density (N_a) was significantly greater (p<.05) than that of ex-smokers without emphysema (ES (w/oE)), but was not significantly different from ex-smokers with CT evidence of emphysema (ES (E)). Internal airway radius (r) and mean linear intercept (L_m) were both significantly smaller in NS than either ES (E) (p<.05 and p<.01 respectively) and ES (w/oE) (p<.0001 and p<.0001 respectively) which were not different from each other. Finally, surface area-to-volume ratio (S/V) was significantly greater in NS than both ES (E) (p<.01) and ES (w/oE) (p<.0001).
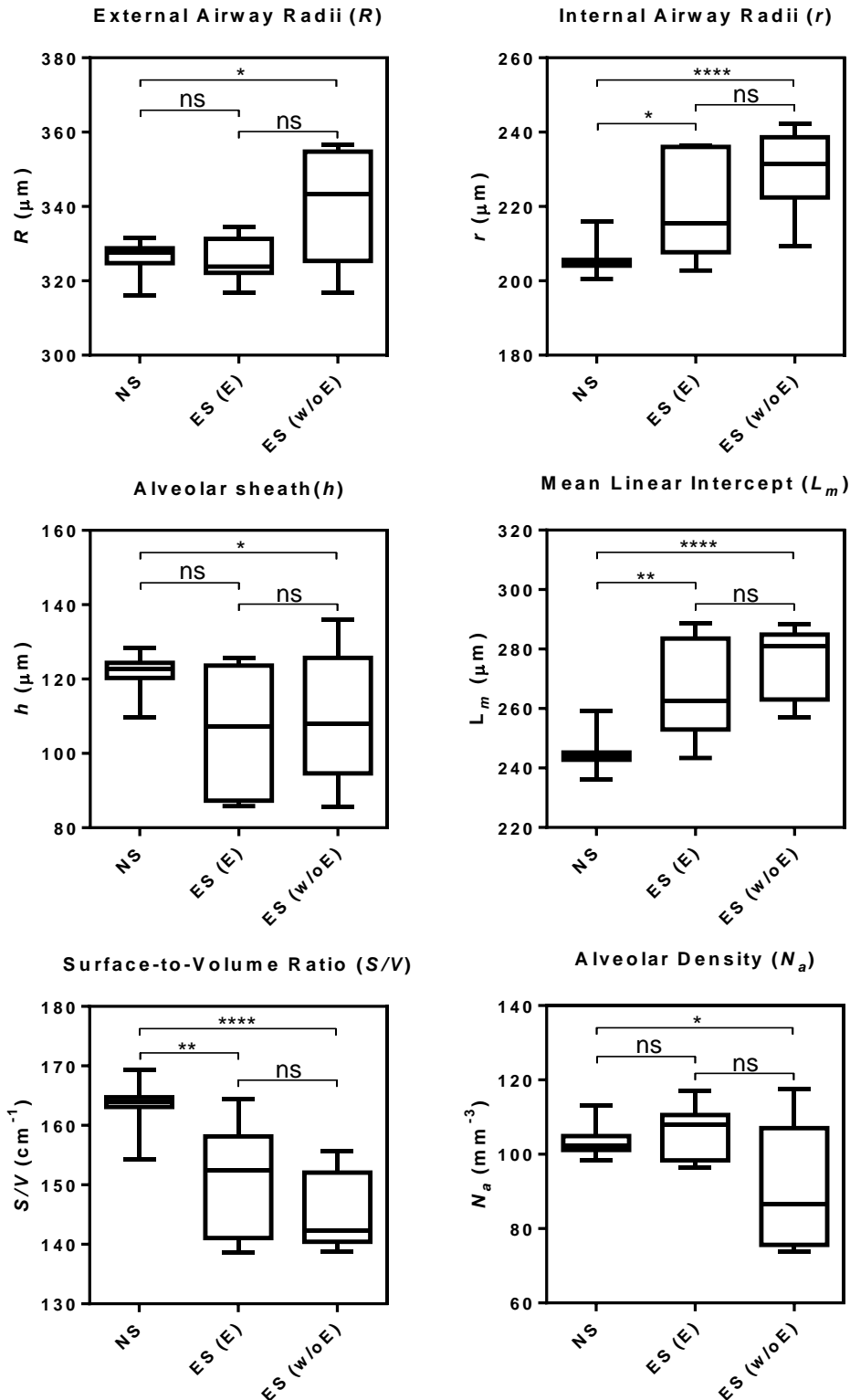
Figure 2-2: ³He Magnetic Resonance Morphometry Measurements. NS, older never-smokers; ES, ex-smokers; E, emphysema; w/o E, without emphysema. For all plots the box extends from the 25th to 75th percentiles while the whiskers are min and max values. Never-smokers, n=40, ex-smokers without emphysema, n=17, and ex-smokers with emphysema, n=7.

*Significance of difference (p<.05) determined using Kruskal-Wallis test along with Dunn's correction.

2.3.3 Morphometry Relationships with Pulmonary Function and CT

The Pearson correlation coefficients between 3He morphometry measurements (R, r, h, Lm, Na, and S/V) and both FEV1/FVC and DLCO for both older never-smokers and ex-smokers are shown in Table 2-3. External airway radius (R) was significantly correlated with FEV1/FVC (r=0.50, p<.05) and DLCO (r=0.58, p<.01) in the ex-smoker group only. Internal airway radius (r) was significantly correlated with FEV1/FVC (r=0.46, p<.01) only in the never-smoker group. Alveolar sheath (h) was not significantly correlated with FEV1/FVC or DLCO in either group. Mean linear intercept (Lm) was significantly correlated with FEV1/FVC (r=0.44, p<.01) and in the never-smoker group only. Analogous to R, alveolar density (Na) was significantly correlated with FEV1/FVC (r=-0.48, p<.05) and DLCO (r=-0.54, p<.01) in the ex-smoker group only. Lastly, similar to r, surface area-to-volume ratio (S/V) was significantly correlated with FEV1/FVC (r=-0.43, p<.01) in the never-smoker group only.

Table 2-3: ^{3}He MR Morphometry Correlations with Pulmonary Function Measures

	Pearson Correlation Coefficients, r (p-value)			
	Older Never-Smokers (n=40)		Ex-Smokers (n=25)	
	FEV_1/FVC	DL_{CO}	FEV_1/FVC	DL_{CO}
R (μm)	ns	ns	**0.50(<.05)**	**0.58(<.01)**
r (μm)	**0.46(<.01)**	ns	ns	ns
h (μm)	ns	ns	ns	ns
L_m (μm)	**0.44(<.01)**	ns	ns	ns
N_a (mm^{-3})	ns	ns	**-0.48(<.05)**	**-0.54(<.01)**
S/V (cm^{-1})	**-0.43(<.01)**	ns	ns	ns

FEV_1, forced expiratory volume in 1 second; FVC, forced vital capacity; DL_{CO}, diffusing capacity of the lung for carbon monoxide percent predicted; R, external airway radius; r, internal airway radius; h, alveolar sheath; L_m, mean linear intercept; N_a, alveolar density; S/V, surface area-to-volume ratio

Figure 2-3 shows linear regressions for the longitudinal (D_L) and transverse (D_T) diffusion coefficients with FEV_1/FVC and DL_{CO} for both older never-smokers and ex-smokers independently. Both D_L and D_T were significant predictors of FEV_1/FVC in the older never-smokers (R^2=0.19, p<.01, R^2=0.13, p<.05) and the ex-smoker groups (R^2=0.31, p<.01, R^2=0.40, p<.01) respectively. D_L was also determined to be a significant predictor

of DL_{CO} in the ex-smoker group (R^2=0.55, p<.0001), but was not a significant predictor in the older-never smoker group. Likewise, D_T was a significant predictor of DL_{CO} in the ex-smoker group (R^2=0.56, p<.0001) only.

● Older never-smokers (NS)   □ Ex-smokers (ES)
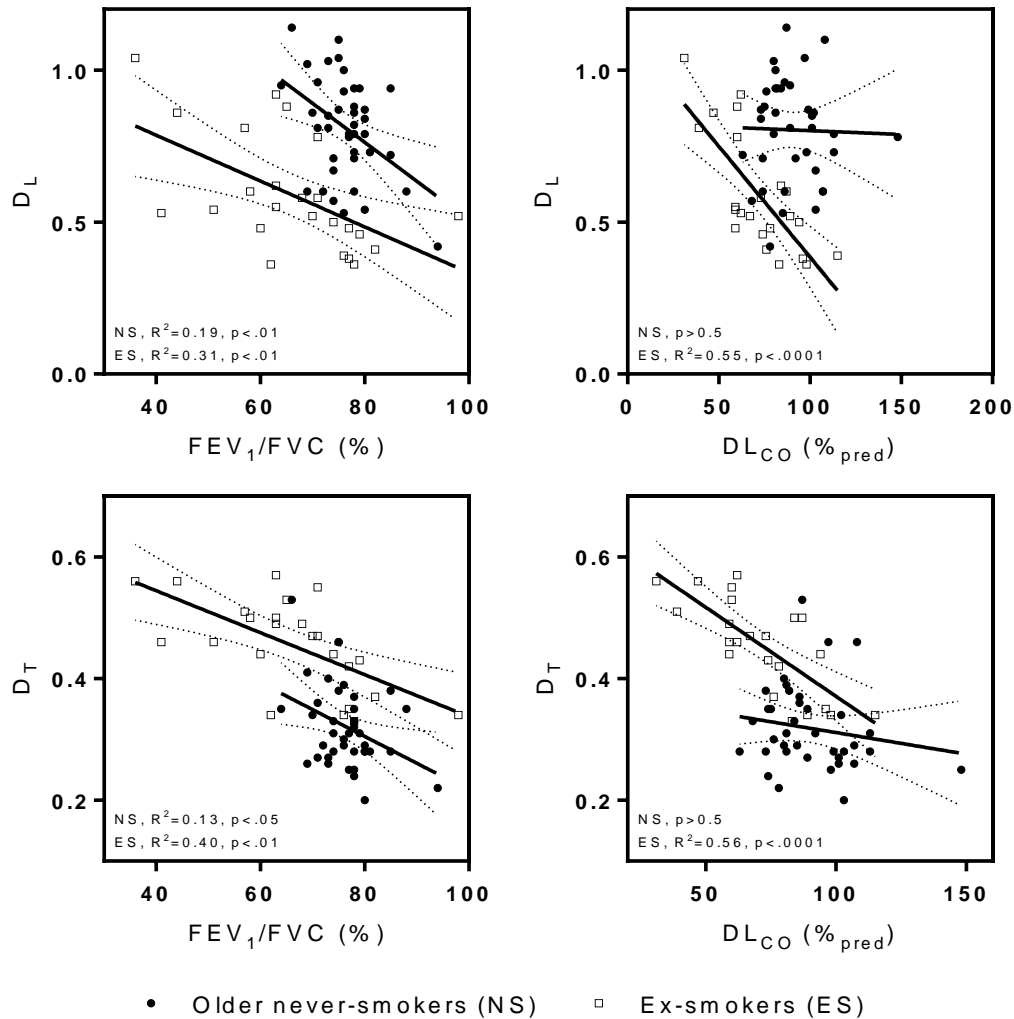
Figure 2-3: Relationships between ³He Diffusion Coefficients with Pulmonary Function Test Measurements. Scatterplots show linear regressions for longitudinal (D_L) and transverse (D_T) diffusion coefficients with FEV_1/FVC and DL_{CO} for both older never-smokers and ex-smokers. Dotted lines indicate the 95% limits of agreement.

2.4   Discussion and Conclusions

To better understand the senile lung and the morphometric changes with age, we evaluated a group of older never-smokers as well as a small group of ex-smokers using hyperpolarized ³He diffusion weighted MRI and made the following observations: 1) older never-smokers appeared to have increased airway radius and mean linear intercept as

compared to literature reported values for younger never-smokers, 2) older never-smokers had significantly lower external and internal airway radius and mean linear intercept, but higher alveolar sheath thickness, alveolar density and surface area-to-volume ratio than ex-smokers, 3) DL_{CO} was not significantly related to morphometry measurements in older never-smokers, while FEV_1/FVC was significantly related, and, 4) both D_L and D_T were significant predictors of FEV_1/FVC in the older never-smokers, but not DL_{CO}.

As expected, older never-smokers had relatively normal pulmonary function measurements based on percent predicted values ($FEV_1/FVC=70\%$, $FEV_1/FVC\%_{pred}=103\%$). When compared to literature reported values for younger never-smokers, we observed increased ADC,[17,33] lower alveolar depth and greater L_m in this group of older never-smokers.[24] The low variance in morphometry measurements among older never-smokers as compared to ex-smokers in this study supports the notion that senile emphysema affects all healthy aging adults to a similar extent when exposed to minimal environmental hazards.

Although elevated compared to literature values for younger never-smokers, the older never-smokers in this study presented with smaller airspaces as compared to the ex-smoker group, which was evident by a lower mean ADC and RA_{950} measurement for all subjects. Further supporting these findings is the fact that older never-smokers had a greater alveolar depth than the ex-smoker group, as well as a higher S/V and lower L_m (Table 2-2 & Figure 2-4). Interestingly, when comparing never-smokers with ex-smokers with, and without, CT evidence of emphysema, these observations remained significant, and we observed the same differences in morphometry measurements with the exception of h, which was not different between the never-smoker and ex-smoker with emphysema groups. Although alveolar depth was not significantly different, this may be due to the small sample size of ex-smokers with emphysema in this study, as the difference between the two groups was not significant by a very fine margin, and may have been exaggerated by an outlier with abnormally large h in the ex-smoker group. As the [3]He lung morphometry technique is used to determine acinar geometry, there are several potential mechanisms for the observed loss of alveolar depth in ex-smokers as compared to healthy older subjects. Emphysematous enlargement of the acinar duct can produce flattening of the alveolus and retraction of the alveolar septa.[34] The increased alveolar depth and S/V in older never-

smokers as compared to younger never-smokers[35] can presumably be attributed to a loss of elastin or change in collagen content, organization and/or distribution with age.[36,37] Moreover, these differences may be explained by the active inflammatory response present in patients with COPD, as would be expected in this group of ex-smokers. This inflammatory component could lead to a thickening of the alveolar walls and septa, effectively reducing the alveolar depth. In addition, the increased acinar duct radius in this group of ex-smokers could indicate an increase in the number and size of pores in the alveolar walls, as they would allow for increased diffusion between adjacent alveoli and acinar ducts.[38] Taken together, these findings suggest that in the senile lung, there may be no active inflammatory component, or change in size or quantity of pores of Kohn (fenestrae) as seen in emphysematous lungs.
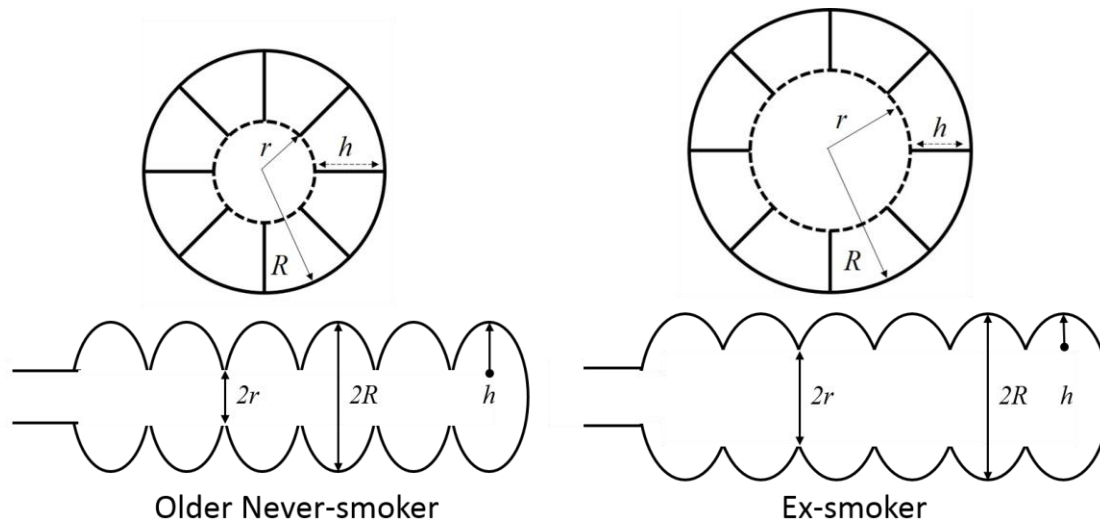
Figure 2-4: Schematic of Airway Parameters for a Representative Older Never-smoker and Ex-smoker. Comparison of internal (r) and external (R) airway radius, as well as alveolar sheath depth (h), showing diminished alveolar depth in ex-smokers.

While DL_{CO} in older never-smokers was not significantly related to any of the microstructural parameters measured, three in particular (r, L_m, and S/V) were significantly related to FEV_1/FVC. The lack of correlation with DL_{CO} in this study is not too surprising as the older never-smokers may have lacked the gross tissue destruction present in COPD-related emphysema that could reduce the gas exchange area sufficiently to alter the diffusive capacity of the lung.[34] Furthermore, the apparent normalcy of DL_{CO} in this group of older never-smoker subjects (approximately 90% predicted) implies that this technique has the potential to be used to detect significant changes in acinar airway geometry, even

in individuals with clinically normal pulmonary function results. By the same token, the especially low RA_{950} values for these older never-smokers, in the presence of elevated L_m as compared to younger never-smokers, implies that the ^{3}He lung morphometry technique has greater sensitivity to early emphysematous changes (airspace enlargement) than does traditional chest CT scoring practices.

Altogether, these findings do not rule out the possibility that environmental factors may play a role in accelerating these changes. For that reason, the technique has considerable potential as an outcome measure for the study of environmental agents such as tobacco smoke or various other pollutants, as well as pharmaceuticals and potential disease therapies or treatments.

In summary, in this small study of older never-smokers, we observed enlarged airspaces as compared to younger never-smokers, while not quite as enlarged as that of ex-smokers. These results, along with a greater observed alveolar density, greater alveolar depth and greater S/V in older never-smokers compared to ex-smokers, support the notion that senile lung does not involve fibrosis or tissue destruction. It implies that the mean airspace size increases with age throughout adult life and is larger in current and past smokers than in healthy never-smokers. The divergence of ex-smokers from older never-smokers is likely a result of accumulated alveolar wall damage and the partial merging of alveoli due to environmental aggravation over time. Ultimately, these results demonstrate that MRI has the potential to replace histology and lung stereology as the gold standard for non-invasive measurements of pulmonary acinus microstructure.

2.5 References

1   Verbeken, E. *et al.* The senile lung. Comparison with normal and emphysematous lungs. 1. Structural aspects. *CHEST Journal* **101**, 793-799 (1992).

2   Frank, N. R., Mead, J. & Ferris, B. G., Jr. The mechanical behavior of the lungs in healthy elderly persons. *The Journal of clinical investigation* **36**, 1680-1687, doi:10.1172/jci103569 (1957).

3   Thurlbeck, W. M. Internal surface area and other measurements in emphysema. *Thorax* **22**, 483-496 (1967).

4   Turner, J. M., Mead, J. & Wohl, M. E. Elasticity of human lungs in relation to age. *Journal of applied physiology (Bethesda, Md. : 1985)* **25**, 664-671 (1968).

5   Janssens, J. P., Pache, J. C. & Nicod, L. P. Physiological changes in respiratory function associated with ageing. *The European respiratory journal* **13**, 197-205 (1999).

6   Fletcher, C. & Peto, R. The natural history of chronic airflow obstruction. *Br. Med. J.* **1**, 1645-1648 (1977).

7   Laennec, R. T. H. & Forbes, J. *A Treatise on the Diseases of the Chest, and on Mediate Auscultation*. (Samuel S. and William Wood, 1834).

8   Hogg, J. C. Pathophysiology of airflow limitation in chronic obstructive pulmonary disease. *Lancet* **364**, 709-721, doi:10.1016/s0140-6736(04)16900-6 (2004).

9   Mayer, E., Blazsik, C. & Rappaport, I. Emphysema and the Lungs of the Aged: A Clinical StudyPreliminary Report. *Chest* **34**, 247-256 (1958).

10   Peterson, D. D., Pack, A. I., Silage, D. A. & Fishman, A. P. Effects of aging on ventilatory and occlusion pressure responses to hypoxia and hypercapnia. *Am. Rev. Respir. Dis.* **124**, 387-391 (1981).

11   Sharma, G. & Goodwin, J. Effect of aging on respiratory system physiology and immunology. *Clin. Interv. Aging* **1**, 253-260 (2006).

12   Young Jr, R. C., Borden, D. L. & Rachal, R. E. Aging of the lung: pulmonary disease in the elderly. *Age* **10**, 138-145 (1987).

13   Kronenberg, R. S. & Drage, C. W. Attenuation of the ventilatory and heart rate responses to hypoxia and hypercapnia with aging in normal men. *J. Clin. Invest.* **52**, 1812 (1973).

14   Yablonskiy, D. A. *et al.* Quantitative in vivo assessment of lung microstructure at the alveolar level with hyperpolarized 3He diffusion MRI. *Proc. Natl. Acad. Sci. U. S. A.* **99**, 3111-3116, doi:10.1073/pnas.052594699 (2002).

15   Yablonskiy, D. A. *et al.* Quantification of lung microstructure with hyperpolarized 3He diffusion MRI. *Journal of applied physiology (Bethesda, Md. : 1985)* **107**, 1258-1265, doi:10.1152/japplphysiol.00386.2009 (2009).

16   Evans, A. *et al.* Anatomical distribution of 3He apparent diffusion coefficients in severe chronic obstructive pulmonary disease. *Journal of magnetic resonance imaging : JMRI* **26**, 1537-1547, doi:10.1002/jmri.21205 (2007).

17   Fain, S. B. *et al.* Detection of age-dependent changes in healthy adult lungs with diffusion-weighted 3He MRI. *Academic radiology* **12**, 1385-1393, doi:10.1016/j.acra.2005.08.005 (2005).

18   Parraga, G. *et al.* Hyperpolarized 3He ventilation defects and apparent diffusion coefficients in chronic obstructive pulmonary disease: preliminary results at 3.0 Tesla. *Investigative radiology* **42**, 384-391, doi:10.1097/01.rli.0000262571.81771.66 (2007).

19   Kirby, M. *et al.* Chronic obstructive pulmonary disease: longitudinal hyperpolarized (3)He MR imaging. *Radiology* **256**, 280-289, doi:10.1148/radiol.10091937 (2010).

20   Parraga, G., Mathew, L., Etemad-Rezai, R., McCormack, D. G. & Santyr, G. E. Hyperpolarized 3He magnetic resonance imaging of ventilation defects in healthy elderly volunteers: initial findings at 3.0 Tesla. *Academic radiology* **15**, 776-785, doi:10.1016/j.acra.2008.03.003 (2008).

21   Salerno, M. *et al.* Emphysema: Hyperpolarized Helium 3 Diffusion MR Imaging of the Lungs Compared with Spirometric Indexes—Initial Experience 1. *Radiology* **222**, 252-260 (2002).

22   Fain, S. B. *et al.* Early Emphysematous Changes in Asymptomatic Smokers: Detection with 3He MR Imaging 1. *Radiology* **239**, 875-883 (2006).

23   Diaz, S. *et al.* Validity of apparent diffusion coefficient hyperpolarized 3He-MRI using MSCT and pulmonary function tests as references. *Eur. J. Radiol.* **71**, 257-263 (2009).

24   Yablonskiy, D. A. *et al.* Quantification of lung microstructure with hyperpolarized 3He diffusion MRI. *Journal of applied physiology (Bethesda, Md. : 1985)* **107**, 1258-1265, doi:10.1152/japplphysiol.00386.2009 (2009).

25   Woods, J. C. *et al.* Hyperpolarized 3He diffusion MRI and histology in pulmonary emphysema. *Magn. Reson. Med.* **56**, 1293-1300 (2006).

26   Quirk, J. D. *et al.* In vivo detection of acinar microstructural changes in early emphysema with 3He lung morphometry. *Radiology* **260**, 866-874 (2011).

27   Miller, M. R. *et al.* Standardisation of spirometry. *Eur Respir J* **26**, 319-338, doi:10.1183/09031936.05.00034805 (2005).

28   Kirby, M. *et al.* Hyperpolarized 3He magnetic resonance functional imaging semiautomated segmentation. *Academic radiology* **19**, 141-152, doi:10.1016/j.acra.2011.10.007 (2012).

29   Gevenois, P. A. *et al.* Comparison of computed density and microscopic morphometry in pulmonary emphysema. *Am J Respir Crit Care Med* **154**, 187-192, doi:10.1164/ajrccm.154.1.8680679 (1996).

30   Sukstanskii, A. L. & Yablonskiy, D. A. In vivo lung morphometry with hyperpolarized 3He diffusion MRI: theoretical background. *J. Magn. Reson.* **190**, 200-210, doi:10.1016/j.jmr.2007.10.015 (2008).

31   Sukstanskii, A. L., Conradi, M. S. & Yablonskiy, D. A. (3)He lung morphometry technique: accuracy analysis and pulse sequence optimization. *J. Magn. Reson.* **207**, 234-241, doi:10.1016/j.jmr.2010.09.005 (2010).

32   Coxson, H. O. *et al.* A quantification of the lung surface area in emphysema using computed tomography. *Am J Respir Crit Care Med* **159**, 851-856, doi:10.1164/ajrccm.159.3.9805067 (1999).

33   Altes, T. A., Mata, J., de Lange, E. E., Brookeman, J. R. & Mugler, J. P., 3rd. Assessment of lung development using hyperpolarized helium-3 diffusion MR imaging. *Journal of magnetic resonance imaging : JMRI* **24**, 1277-1283, doi:10.1002/jmri.20723 (2006).

34   Hartroft, W. S. The Microscopic Diagnosis of Pulmonary Emphysema. *Am. J. Pathol.* **21**, 889-903 (1945).

35   Quirk, J. D., Chang, Y. V. & Yablonskiy, D. A. In vivo lung morphometry with hyperpolarized He diffusion MRI: Reproducibility and the role of diffusion-sensitizing gradient direction. *Magn. Reson. Med.*, doi:10.1002/mrm.25241 (2014).

36   West, J. B. Distribution of mechanical stress in the lung, a possible factor in localisation of pulmonary disease. *Lancet* **1**, 839-841 (1971).

37   Sobin, S. S., Fung, Y. C. & Tremer, H. M. Collagen and elastin fibers in human pulmonary alveolar walls. *Journal of applied physiology (Bethesda, Md. : 1985)* **64**, 1659-1675 (1988).

38   Nagai, A. & Thurlbeck, W. M. Scanning electron microscopic observations of emphysema in humans. A descriptive study. *Am. Rev. Respir. Dis.* **144**, 901-908, doi:10.1164/ajrccm/144.4.901 (1991).

3   CHAPTER 3: CONCLUSIONS AND FUTURE WORK

In this final chapter, I will provide an overview and summary of the important findings and conclusions of Chapter 2. I will also address the limitations of the hyperpolarized gas MRI lung morphometry technique presented and provide some potential solutions. Finally, based on the findings and limitations discussed, I will outline a roadmap for future studies.

3.1   Overview and Summary

Senile emphysema is characterized by distal airway enlargement without obvious fibrosis or alveolar wall destruction.[1] Other structural components of senile lung include the loss of elastic fibers, thickening of alveolar walls[1], and diminished pulmonary elastic recoil.[2-4] As patients do not present with the clinical symptoms of emphysema, senile emphysema is more correctly identified as senile lung.[5] Emphysema, as linked to chronic obstructive pulmonary disease (COPD), is unique from senile lung in that the presence of fibrosis and tissue destruction leads to deformation of the alveoli.[6]

Subjects with senile lung appear to have sufficient lung function for their normal day-to-day activities,[7] however these changes tend to increase the risk of breathlessness and respiratory failure in the elderly when compromised. Further complications in health result when these changes are concomitant with cardiac impairment and/or respiratory infection.[8-10] These age-dependent structural and functional changes can reduce sensitivity of the respiratory centres to hypoxia or hypercapnia, resulting in a diminished ventilatory response in cases of heart failure or airway obstruction.[8,11,12] As a consequence of the reduction in supporting tissues and tethering forces around the airways with age, there is a tendency for the smaller airways to collapse. Accordingly, premature closure of these airways becomes common during normal tidal breathing.

Stereological techniques have historically been used to measure pulmonary morphometry, and as such the technique has become the gold standard for exploring the structural changes associated with various pulmonary diseases. Emphysema has commonly been studied using these techniques, however most work has ignored the effects of septal destruction,

and looked solely at airspace enlargement.[13] Alternatively, micro–CT has rapidly emerged as an imaging technique with the potential to measure lung microstructure on length scales much smaller than previously possible with clinical CT scanners. This technology consequently offers the ability to analyze acinar morphometry without the need for physical segmentation, thus maintaining an undamaged, three-dimensional (3-D) structure.[14] Unfortunately, due to the long exposure time and high dose associated with this technique, scanning living organisms is difficult, if not altogether impossible. Unfortunately, with both of these techniques, choice of inflation and fixation techniques introduce a number of errors and biases.[15] As such, a non-invasive imaging method that can evaluate both lung structure and function without the use of ionizing radiation or tissue fixation/preparation is required.

Hyperpolarized inhaled noble gas MRI provides non-invasive measurements of lung function and structure [16-21] showing those regions of the lung that participate in ventilation and those that do not.[21,22] In addition, the MRI ADC for an inhaled gas is sensitive to changes in the lung microstructure and airspace size correlating well with age [19], spirometry [23], DL_{CO} [24], and CT measurements of emphysema [25]. Previous studies have shown a close agreement between alveolar parameters obtained using the ^{3}He MRI lung morphometry technique and those measurements found by direct histological analysis.[26]

In Chapter 2 we quantitatively evaluated a group of 42 older never-smokers and 25 ex-smokers using hyperpolarized ^{3}He diffusion weighted MRI. The acinar duct morphometry results were found to be within the physiological range reported in literature. Calculated values of internal (r) and external (R) airway radius as well as mean linear intercept (L_m) for individual subjects were similar with low variance. Results showed that MRI measurements of lung airspace size in healthy older never-smokers were elevated compared to previous results reported in younger never-smokers. Such results are consistent with senile emphysematous changes to healthy parenchyma that accompanies aging. Furthermore, this study showed that there was a greater observed alveolar density, greater alveolar depth and greater surface area-to-volume ratio in older never-smokers as compared to ex-smokers, supporting the notion that senile lung does not involve fibrosis

or tissue destruction. These results suggest MRI has the potential to replace lung stereology as the gold standard for measuring pulmonary acinus microstructure.

3.2 Limitations of Current Work

A number of limitations currently affect the potential clinical translation of this technique. Firstly, ^{3}He MRI requires unique expertise and equipment. There is an extremely limited supply of helium gas, making further follow-up studies and clinical implementation of this technique questionable. With regards to the polarization itself, the process is dependent on expensive equipment that relies heavily on highly skilled operators who can handle, prepare, and administer the gas in a time-sensitive manner.

In addition to the physical limitations, there is still room for improvement in modelling pulmonary morphometry. As was evident in this study, algorithm optimization is still required as not all diffusion data could be successfully fit to the model each subject. Furthermore, although more time efficient than lung stereology, MRI morphometry still requires manual observer interaction and is computationally intense. The model itself typically requires between 2-3 hours of runtime per subject per slice, depending on the complexity of the data. Fortunately, multiple instances of the program can be run in parallel, significantly shortening the overall processing time for large data sets.

Specific to this technique, the morphological equations are quantitatively valid in the physiologically important range of the airways parameters characteristic of healthy lungs and those with mild emphysema. However, when acinar airways deviate significantly from this range, in the case of severe emphysema, the "cylindrical" model is expected to fail. In lungs with advanced emphysema, our results might provide only the "apparent" diffusion characteristics. Furthermore, for lungs with substantial degeneration of the acinar walls, the model requires further generalization in order to account for the expansion of large air cavities in which ^{3}He diffusion is much less restricted. A further limitation results from the assumption at the base of the diffusion/morphometry relationship (*R, r,* and *h*) which presumes that the diffusing ^{3}He atoms cannot penetrate through alveolar walls. In reality though, alveolar walls have pores, however their effects on D_L and D_T are considered negligible in healthy subjects due to the small number of microscopic (<10 μm) pores

present.[27] In the emphysematous lung, this assumption weakens, as more pores of variable size (>20 μm) occur in alveolar walls, ultimately increasing the transverse and longitudinal ADCs .[28] These effects fall beyond the scope of this study, and will need to be addressed in future studies. All things considered, these measures are still capable of providing a wealth of information regarding emphysematous progression when interpreted in the context of disease severity.

One other limitation of this study is the lack of data collected from other imaging modalities or techniques in conjunction with ^{3}He MRI. Both micro-CT and stereological data could have been used to validate the measurements acquired using this technique, however these procedures were infeasible due to their highly invasive nature and would have required biopsies or cadaveric samples.

3.3   Future Work

The results and discussions presented in this thesis provide some important insights regarding the use and applicability of the hyperpolarized ^{3}He morphometry technique in developing a deeper understanding of the structural and functional changes that occur during the normal lung aging process. In order for this technique to supplant the current invasive gold standard of lung stereology, there is a need for further development into the automation and removal of all user interaction with processing the diffusion weighted image data.

Additionally, due to the limited availability and high cost of ^{3}He gas, its clinical translation will become increasingly difficult in the coming years. As such, future studies comparing ^{3}He-derived morphometry measurements with ^{129}Xe-derived measurements will be of great importance. ^{129}Xe gas is more abundant and as such substantially cheaper than ^{3}He, hence making it a more realistic option as an imaging agent in clinical applications. Recent studies have begun assessing pulmonary microstructure using ^{129}Xe in healthy young subjects and those with mild COPD[29], however, due to the differences in the physical properties between the two gases, it is not known how these results would differ when assessing an older never-smoker population. Furthermore, application of a ^{129}Xe diffusion weighted technique will provide unique information on the relationship between lung

morphometry and pulmonary perfusion. The unique property of ^{129}Xe to perfuse from the acinus into the surrounding capillaries would provide a better understanding of the relative stability of DL_{CO} with age even in the presence of senile emphysema.

Finally, while this work has focused on mean values of ^{3}He diffusion morphometry values, this approach ignores a major benefit of the imaging technique, namely the ability to acquire regional pulmonary information or data from follow-up texture analysis information. The heterogeneity of disease across the lung has been shown previously in subjects with asthma and COPD, and thus having a regional understanding of senile lung may help elucidate the nature and potential patterns present in the age-related increase in airspace. Future efforts to analyze this distribution would likely be informative, potentially enabling identification of different senile lung phenotypes based on patterns of lung abnormalities.

3.4 References

1 Verbeken, E. *et al.* The senile lung. Comparison with normal and emphysematous lungs. 1. Structural aspects. *CHEST Journal* **101**, 793-799 (1992).

2 Frank, N. R., Mead, J. & Ferris, B. G., Jr. The mechanical behavior of the lungs in healthy elderly persons. *The Journal of clinical investigation* **36**, 1680-1687, doi:10.1172/jci103569 (1957).

3 Thurlbeck, W. M. Internal surface area and other measurements in emphysema. *Thorax* **22**, 483-496 (1967).

4 Turner, J. M., Mead, J. & Wohl, M. E. Elasticity of human lungs in relation to age. *Journal of applied physiology (Bethesda, Md. : 1985)* **25**, 664-671 (1968).

5 Laennec, R. T. H. & Forbes, J. *A Treatise on the Diseases of the Chest, and on Mediate Auscultation*. (Samuel S. and William Wood, 1834).

6 Hogg, J. C. Pathophysiology of airflow limitation in chronic obstructive pulmonary disease. *Lancet* **364**, 709-721, doi:10.1016/s0140-6736(04)16900-6 (2004).

7 Mayer, E., Blazsik, C. & Rappaport, I. Emphysema and the Lungs of the Aged: A Clinical StudyPreliminary Report. *Chest* **34**, 247-256 (1958).

8 Peterson, D. D., Pack, A. I., Silage, D. A. & Fishman, A. P. Effects of aging on ventilatory and occlusion pressure responses to hypoxia and hypercapnia. *Am. Rev. Respir. Dis.* **124**, 387-391 (1981).

9 Sharma, G. & Goodwin, J. Effect of aging on respiratory system physiology and immunology. *Clin. Interv. Aging* **1**, 253-260 (2006).

10 Young Jr, R. C., Borden, D. L. & Rachal, R. E. Aging of the lung: pulmonary disease in the elderly. *Age* **10**, 138-145 (1987).

11 Janssens, J. P., Pache, J. C. & Nicod, L. P. Physiological changes in respiratory function associated with ageing. *Eur Respir J* **13**, 197-205 (1999).

12 Kronenberg, R. S. & Drage, C. W. Attenuation of the ventilatory and heart rate responses to hypoxia and hypercapnia with aging in normal men. *J. Clin. Invest.* **52**, 1812 (1973).

13 Fehrenbach, H. Animal models of pulmonary emphysema: a stereologist's perspective. *European Respiratory Review* **15**, 136-147 (2006).

14 Vasilescu, D. M. *et al.* Stereological assessment of mouse lung parenchyma via nondestructive, multiscale micro-CT imaging validated by light microscopic histology. *J. Appl. Physiol.* **114**, 716-724 (2013).

15   Litzlbauer, H. D. *et al.* Synchrotron-based micro-CT imaging of the human lung acinus. *Anat Rec (Hoboken)* **293**, 1607-1614, doi:10.1002/ar.21161 (2010).

16   Yablonskiy, D. A. *et al.* Quantitative in vivo assessment of lung microstructure at the alveolar level with hyperpolarized 3He diffusion MRI. *Proc. Natl. Acad. Sci. U. S. A.* **99**, 3111-3116, doi:10.1073/pnas.052594699 (2002).

17   Yablonskiy, D. A. *et al.* Quantification of lung microstructure with hyperpolarized 3He diffusion MRI. *Journal of applied physiology (Bethesda, Md. : 1985)* **107**, 1258-1265, doi:10.1152/japplphysiol.00386.2009 (2009).

18   Evans, A. *et al.* Anatomical distribution of 3He apparent diffusion coefficients in severe chronic obstructive pulmonary disease. *Journal of magnetic resonance imaging : JMRI* **26**, 1537-1547, doi:10.1002/jmri.21205 (2007).

19   Fain, S. B. *et al.* Detection of age-dependent changes in healthy adult lungs with diffusion-weighted 3He MRI. *Academic radiology* **12**, 1385-1393, doi:10.1016/j.acra.2005.08.005 (2005).

20   Parraga, G. *et al.* Hyperpolarized 3He ventilation defects and apparent diffusion coefficients in chronic obstructive pulmonary disease: preliminary results at 3.0 Tesla. *Investigative radiology* **42**, 384-391, doi:10.1097/01.rli.0000262571.81771.66 (2007).

21   Kirby, M. *et al.* Chronic obstructive pulmonary disease: longitudinal hyperpolarized (3)He MR imaging. *Radiology* **256**, 280-289, doi:10.1148/radiol.10091937 (2010).

22   Parraga, G., Mathew, L., Etemad-Rezai, R., McCormack, D. G. & Santyr, G. E. Hyperpolarized 3He magnetic resonance imaging of ventilation defects in healthy elderly volunteers: initial findings at 3.0 Tesla. *Academic radiology* **15**, 776-785, doi:10.1016/j.acra.2008.03.003 (2008).

23   Salerno, M. *et al.* Emphysema: Hyperpolarized Helium 3 Diffusion MR Imaging of the Lungs Compared with Spirometric Indexes—Initial Experience 1. *Radiology* **222**, 252-260 (2002).

24   Fain, S. B. *et al.* Early Emphysematous Changes in Asymptomatic Smokers: Detection with 3He MR Imaging 1. *Radiology* **239**, 875-883 (2006).

25   Diaz, S. *et al.* Validity of apparent diffusion coefficient hyperpolarized 3He-MRI using MSCT and pulmonary function tests as references. *Eur. J. Radiol.* **71**, 257-263 (2009).

26   Yablonskiy, D. A. *et al.* Quantification of lung microstructure with hyperpolarized 3He diffusion MRI. *Journal of applied physiology (Bethesda, Md. : 1985)* **107**, 1258-1265, doi:10.1152/japplphysiol.00386.2009 (2009).

27   Nagai, A., Thurlbeck, W. M. & Konno, K. Responsiveness and variability of airflow obstruction in chronic obstructive pulmonary disease. Clinicopathologic correlative studies. *Am J Respir Crit Care Med* **151**, 635-639, doi:10.1164/ajrccm.151.3.7881649 (1995).

28   Nagai, A. & Thurlbeck, W. M. Scanning electron microscopic observations of emphysema in humans. A descriptive study. *Am. Rev. Respir. Dis.* **144**, 901-908, doi:10.1164/ajrccm/144.4.901 (1991).

29   Ouriadov, A. *et al.* Lung morphometry using hyperpolarized (129) Xe apparent diffusion coefficient anisotropy in chronic obstructive pulmonary disease. *Magn. Reson. Med.* **70**, 1699-1706, doi:10.1002/mrm.24595 (2013).

4 APPENDIX

Appendix A: Health Science Research Ethics Board Approval (ROB0003)

Office of Research Ethics

Use of Human Subjects - Ethics Approval Notice

Principal Investigator: Dr. G. Parraga	
Review Number: 17396	**Review Level:** Full Board
Review Date: September 14, 2010	**Approved Local # of Participants:** 18
Protocol Title: Longitudinal 3He Magnetic Resonance Imaging of Health Lung	
Department and Institution: Imaging, Robarts Research Institute	
Sponsor: CIHR-CANADIAN INSTITUTE OF HEALTH RESEARCH	
Ethics Approval Date: November 09, 2010	**Expiry Date:** September 30, 2014
Documents Reviewed and Approved: UWO Protocol (including instruments noted in Section 8.1), Letter of Information an Consent Form dated Sept. 27, 2010 version 2, and Advertisement.	
Documents Received for Information: Clinical Study Protocol Version #1 27 August 2010; IB NC100182-Inhalation (Hyperpolarised 3HE) 6th edition 09 Sep 05; NC1000182 IB April 7, 2009; Product Monograph Ventolin HFA	

This is to notify you that The University of Western Ontario Research Ethics Board for Health Sciences Research Involving Hur Subjects (HSREB) which is organized and operates according to the Tri-Council Policy Statement: Ethical Conduct of Research Involving Humans and the Health Canada/ICH Good Clinical Practice Practices: Consolidated Guidelines; and the applicable la regulations of Ontario has reviewed and granted approval to the above referenced study on the approval date noted above. The membership of this REB also complies with the membership requirements for REB's as defined in Division 5 of the Food and D Regulations.

he ethics approval for this study shall remain valid until the expiry date noted above assuming timely and acceptable responses SREB's periodic requests for surveillance and monitoring information. If you require an updated approval notice prior to that you must request it using the UWO Updated Approval Request Form.

During the course of the research, no deviations from, or changes to, the protocol or consent form may be initiated without prior written approval from the HSREB except when necessary to eliminate immediate hazards to the subject or when the change(s) i only logistical or administrative aspects of the study (e.g. change of monitor, telephone number). Expedited review of minor change(s) in ongoing studies will be considered. Subjects must receive a copy of the signed information/consent documentation

Investigators must promptly also report to the HSREB:

  a) changes increasing the risk to the participant(s) and/or affecting significantly the conduct of the study;
  b) all adverse and unexpected experiences or events that are both serious and unexpected;
 c) new information that may adversely affect the safety of the subjects or the conduct of the study.

If these changes/adverse events require a change to the information/consent documentation, and/or recruitment advertisement, t newly revised information/consent documentation, and/or advertisement, must be submitted to this office for approval.

Members of the HSREB who are named as investigators in research studies, or declare a conflict of interest, do not participate i discussion related to, nor vote on, such studies when they are presented to the HSREB.

Chair of HSREB: Dr. Joseph
FDA Ref. #: IRB 00

Ethics Officer to Contact for Further Information

Appendix B: Health Science Research Ethics Board Approval (ROB0018)
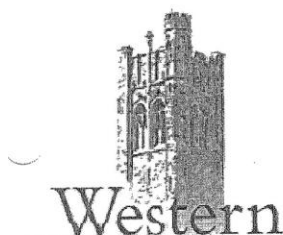
Office of Research Ethics

Use of Human Subjects - Ethics Approval Notice

Principal Investigator: Dr. G. Parraga
Review Number: 15930　　　　　　　　**Review Level:** Full Board
Review Date: February 10, 2009

Protocol Title: Longitudinal Study of Helium-3 Magnetic Resonance Imaging of COPD
Department and Institution: Diagnostic Radiology & Nuclear Medicine, Robarts Research Institute
Sponsor: INTERNAL RESEARCH FUND-UWO
Ethics Approval Date: May 25, 2009　　　　　　**Expiry Date:** November 30, 2013
Documents Reviewed and Approved: UWO Protocol, Letter of information & consent form for Patients dated March 26/09
　　　　Letter of information & consent form for Healthy Volunteers dated March 26/09
Documents Received for Information: Protocol, January 27, 2009; IB, ed 6, 09 Sep. 05

This is to notify you that The University of Western Ontario Research Ethics Board for Health Sciences Research Involving Hum
Subjects (HSREB) which is organized and operates according to the Tri-Council Policy Statement: Ethical Conduct of Research
Involving Humans and the Health Canada/ICH Good Clinical Practice Practices: Consolidated Guidelines; and the applicable law
regulations of Ontario has reviewed and granted approval to the above referenced study on the approval date noted above. The
membership of this REB also complies with the membership requirements for REB's as defined in Division 5 of the Food and Dr
Regulations.

The ethics approval for this study shall remain valid until the expiry date noted above assuming timely and acceptable responses
HSREB's periodic requests for surveillance and monitoring information. If you require an updated approval notice prior to that t
you must request it using the UWO Updated Approval Request Form.

During the course of the research, no deviations from, or changes to, the protocol or consent form may be initiated without prior
written approval from the HSREB except when necessary to eliminate immediate hazards to the subject or when the change(s) in
only logistical or administrative aspects of the study (e.g. change of monitor, telephone number). Expedited review of minor
change(s) in ongoing studies will be considered. Subjects must receive a copy of the signed information/consent documentation.

Investigators must promptly also report to the HSREB:

　　a) changes increasing the risk to the participant(s) and/or affecting significantly the conduct of the study;
　　b) all adverse and unexpected experiences or events that are both serious and unexpected;
　　c) new information that may adversely affect the safety of the subjects or the conduct of the study.

If these changes/adverse events require a change to the information/consent documentation, and/or recruitment advertisement, th
newly revised information/consent documentation, and/or advertisement, must be submitted to this office for approval.

Members of the HSREB who are named as investigators in research studies, or declare a conflict of interest, do not participate in
discussion related to, nor vote on, such studies when they are presented to the HSREB.

　　　　　　　　　　　　　　　　　　　　　　　　　Chair of HSREB: Dr. Joseph

_____
Ethics Officer to Contact for Further Information

Appendix C: Copyright Material and Permission for Figures 1-6, 1-7, and 1-8

**AMERICAN COLLEGE OF CHEST PHYSICIANS LICENSE
TERMS AND CONDITIONS**

Mar 16, 2015

This is a License Agreement between Gregory A Paulin ("You") and American College of Chest Physicians ("American College of Chest Physicians") provided by Copyright Clearance Center ("CCC"). The license consists of your order details, the terms and conditions provided by American College of Chest Physicians, and the payment terms and conditions.

All payments must be made in full to CCC. For payment instructions, please see information listed at the bottom of this form.

License Number	3590840235668
License date	Mar 16, 2015
Licensed content publisher	American College of Chest Physicians
Licensed content publication	CHEST
Licensed content title	The senile lung. Comparison with normal and emphysematous lungs. 1. Structural aspects.
Licensed content author	Verbeken, E K; Cauberghs, M; Mertens, I et. al.
Licensed content date	Mar 1, 1992
Volume number	101
Issue number	3
Type of Use	Thesis/Dissertation
Requestor type	individual
Format	print and electronic
Portion	figures/tables/images
Number of figures/tables/images	1
Will you be translating?	no
Content will be altered	None
Order reference number	None
Title of your thesis / dissertation	Non-Invasive Quantification Of Alveolar Morphometry Measurements In Older Never-Smokers
Expected completion date	Apr 2015
Estimated size (number of pages)	90
Total	0.00 CAD
Terms and Conditions	

STANDARD TERMS AND CONDITIONS FOR REPRODUCTION OF MATERIAL

RightsLink®

Title: Quantitative microscopy of the lung: a problem-based approach. Part 2: stereological parameters and study designs in various diseases of the respiratory tract

Author: Christian Mühlfeld ,Matthias Ochs

Publication: Am J Physiol-Lung, Cellular, and Molecular Physiology

Publisher: The American Physiological Society

Date: Mar 13, 2015

Copyright © 2015, The American Physiological Society

Permission Not Required

Permission is not required for this type of use.

BACK   CLOSE WINDOW

RADIOLOGICAL SOCIETY OF NORTH AMERICA
820 JORIE BLVD, OAK BROOK, IL 60523
TEL 1-630-571-2670 FAX 1-630-571-7837
RSNA.ORG

100 YEARS RSNA®

March 17, 2015

Dear Gregory Paulin:

The Radiological Society of North America (RSNA®) is pleased to grant you permission to reproduce the following figures in print and electronic formats for educational, non-profit use in your thesis, provided you give full credit to the authors of the original publication.

> Figures 1b, 2b
> Watz H, Breithecker A, Rau W S, et al. Micro-CT of the human lung: Imaging of alveoli and virtual endoscopy of an alveolar duct in a normal lung and in a lung with centrilobular emphysema—initial observations. *Radiology* 2005;236:1053-1058.

This permission is a one-time, non-exclusive grant for English-language use and is exclusively limited to the usage stated and underlined above. The requestor guarantees to reproduce the material as originally published. Permission is granted under the condition that a full credit line is prominently placed (i.e. author name(s), journal name, copyright year, volume #, inclusive pages and copyright holder).

This permission becomes effective upon receipt of this signed contract. Please sign a copy of this agreement, return a signed copy to me and retain a copy for your files. Thank you for your interest in our publication.

[Print Name]:

SIGNATURE: Date: March 17, 2015

Sincerely,

5   CURRICULUM VITAE

Gregory Paulin, B.M.Sc., B.A.

Imaging Research Laboratories
Robarts Research Institute

EDUCATION

09/13-present Master of Science (*Candidate*)
Department of Medical Biophysics, Robarts Research Institute
The University of Western Ontario, London, Ontario, Canada
Supervisor: Dr. Grace Parraga

09/08-08/13   Bachelor of Medical Science (BMSc) with Distinction
Honours Specialization in Medical Science
The University of Western Ontario, London, Ontario, Canada

09/10-08/13   Bachelor of Arts (BA) with Distinction
Honours Business Administration
The Richard Ivey School of Business, London, Ontario, Canada

POSITIONS

05/13-08/13   Summer Research Student
Department of Medical Biophysics
The University of Western Ontario, London, Ontario, Canada
Supervisor: Dr. Grace Parraga

05/12-08/12   Summer Research Student
Department of Surgery and Oncology
Juravinski Cancer Centre, McMaster University, Hamilton, Ontario,
Canada
Supervisor: Dr. Helga Duivenvoorden

05/11-08/11   Summer Research Student
Department of Surgery and Oncology
Juravinski Cancer Centre, McMaster University, Hamilton, Ontario,
Canada
Supervisor: Dr. Helga Duivenvoorden

05/10-08/10   Summer Research Assistant
Department of Surgery and Oncology
Juravinski Cancer Centre, McMaster University, Hamilton, Ontario, Canada
Supervisor: Dr. Jehonathan Pinthus

05/09-08/09   Summer Research Assistant
Department of Surgery and Oncology
Juravinski Cancer Centre, McMaster University, Hamilton, Ontario, Canada
Supervisor: Dr. Jehonathan Pinthus

01/07-08/09   Barista/Sales Associate
Second Cup, Hamilton, Ontario, Canada
Manager: Terry Lee

ACADEMIC AWARDS, SCHOLARSHIPS, and DISTINCTIONS

05/14   Ontario Graduate Scholarship
Awarded to outstanding graduate students in the province of Ontario; $15,000
Provincial

03/14 Problems   American Thoracic Society Abstract Scholarship- Assembly on Clinical

Awarded to outstanding abstract submissions to the ATS International Conference; $500
International

09/13   Western Graduate Research Scholarship
Awarded to a full-time student who has maintained an average 80% or above.
Institutional

04/12-04/13   Dean's Honour Roll
Awarded to a full-time student who has maintained an average 80% or above.
Institutional

04/11   Dean's Honour Roll
Awarded to a full-time student at the Richard Ivey School of Business who has placed in the top quartile of the program.
Institutional

04/09-04/10   Dean's Honour Roll

Awarded to a full-time student who has maintained an average 80% or above.
Institutional

06/09   ArcelorMittal University Scholarship
Awarded to a full-time student who has exhibited both academic and extracurricular success.

09/08   Western Entrance Scholarship
Awarded to a full-time student who has maintained an average 80% or above.
Institutional

06/08   Principal's Scholarship for Academic Excellence
Awarded for overall academic success in all four years of high school (3 students awarded total).

PUBLICATIONS and PRESENTATIONS

A. Refereed Journal Manuscripts (4 published)

Published (4)

1. **Paulin G**, Svenningsen S, Jobse B, Kirby M, McCormack DG, Lewis JF, Parraga G. Differences in Hyperpolarized ^{3}He Ventilation Imaging after Four-years in Adults with Cystic Fibrosis. *Journal of Magnetic Resonance Imaging.* 2014; doi: 10.1002/jmri.24744. [Epub ahead of print].

2. Sheikh K, **Paulin G**, Svenningsen S, Kirby M, Paterson NAM, McCormack DG, and Parraga G. Pulmonary Ventilation Defects in Older Never-Smokers. *Journal of Applied Physiology.* 2014; 117(3):297-306.

3. Duivenvoorden WC, Beatty LK, Lhotak S, Hill B, Mak I, **Paulin G**, Gallino D, Popovic S, Austin RC and Pinthus JH. Underexpression of tumour suppressor LKB1 in clear cell renal cell carcinoma is common and confers growth advantage in vitro and in vivo. *British Journal of Cancer* 2013; 108(2):327-33.

4. Whelan KF, Lu JP, Fridman E, Wolf A, Honig A, **Paulin G**, Klotz L and Pinthus JH. What can surrogate tissues tell us about the oxidative stress status of the prostate? A hypothesis-generating in-vivo study. *PloS one* 2010; 5(12):e15880.

B. Conference Proceedings

Oral Presentation (5)

1. Svenningsen, S; **Paulin, G**; Kirby, M; Kanhere, N; Etemad-Rezai, R; McCormack, DG; Parraga, G; *Pulmonary Functional MRI to Phenotype COPD and Evaluate Treatment Efficacy: Intermediate Endpoints and Predictors of Efficacy when Conventional endpoints fail? International Society for Magnetic Resonance in Medicine* 2014

2. **Paulin, G**; Svenningsen, S; Mohan, S; Jobse, BN; Kirby, M; Lewis, JF; Parraga, G; *Longitudinal Hyperpolarized ^{3}He Magnetic Resonance Imaging of Adult Cystic Fibrosis: Pilot Study results. Imaging Network of Ontario* 2014

3. Stankiewicz, M; Svenningsen, S; **Paulin, G**; Maksym, G; McCormack, DG; Parraga, G; *Respiratory Resistance in Bronchiectasis and COPD using the Forced Oscillation Technique. American Thoracic Society* 2014

4. Svenningsen, S; **Paulin, G**; Pike, D; Mohan, S; McCormack, DG; Parraga G; *Pulmonary Functional Imaging of Bronchiectasis: A First Look at Ventilation Abnormalities and their Relationship with Pulmonary Function and Symptoms. American Thoracic Society* 2014

5. Svenningsen, S; **Paulin, G**; Pike, D; Mohan, S; McCormack, DG; Parraga G; *Pulmonary Functional Imaging of Bronchiectasis: A First Look at Ventilation Abnormalities and their Relationship with Pulmonary Function and Symptoms. Imaging Network of Ontario* 2014

Accepted Posters (7)

1. **Paulin, G**; Sheikh, K; McCormack, DG; Parraga, G; *Differences in Pulmonary Structure and Function in Healthy Elderly Never-smokers after Two Years. American Thoracic Society* 2015

2. Sheikh, K; **Paulin, G**; Svenningsen, S; McCormack, DG; Neder, JA; Parraga, G; *How do Exercise Responses Relate to 3He Magnetic Resonance Imaging Apparent Diffusion Coefficients in Older Never-Smokers? American Thoracic Society* 2015

3. Svenningsen, S; Capaldi, D; Bluemke, E; **Paulin, G**; Davis, C; Sheikh, K; McCormack, DG; Parraga, G; *Lung Clearance Index and Hyperpolarized 3He MRI Ventilation Heterogeneity Measurements in Non-CF Bronchiectasis and COPD. American Thoracic Society* 2015

4. Bluemke, E; Svenningsen, S; **Paulin, G**; Sheikh, K; McCormack, DG; Parraga, G; *Relationship of Ventilation Heterogeneity in the Conducting and Acinar Airway Zones with 3He MRI in Elderly Never-Smokers. American Thoracic Society* 2015

5. **Paulin, G**; Svenningsen, S; Lewis, JF; McCormack, DG; Parraga, G; *Hyperpolarized ^{3}He MRI Ventilation Abnormalities of Cystic Fibrosis and Non-Cystic Fibrosis Bronchiectasis. American Thoracic Society* 2014

6. **Paulin, G**; Svenningsen, S; Mohan, S; Jobse, BN; Kirby, M; Lewis, JF; Parraga, G; *Longitudinal Hyperpolarized ^{3}He Magnetic Resonance Imaging of Adult Cystic Fibrosis: Pilot Study results. American Thoracic Society* 2014

7. Capaldi, D; Sheikh, K; **Paulin, G**; Svenningsen, S; Coxson, HO; McCormack, DG; Parraga, G; *Conventional non-contrast MRI of Ventilation Abnormalities in Bronchiectasis: New Tools and Measurements for an old Disease. American Thoracic Society* 2014

8. Mohan, S; **Paulin, G**; Svenningsen, S; Lewis, JF; Parraga, G; *Can Pulmonary Functional imaging guide therapy of Cystic Fibrosis Pulmonary Exacerbations? American Thoracic Society* 2014

9. Svenningsen, S; **Paulin, G**; McCormack, DG; Parraga, G*; Ventilation Abnormalities in Chronic Bronchitis and Bronchiectasis: Is there a difference? American Thoracic Society* 2014

10. Capaldi, D; Sheikh, K; **Paulin, G**; Svenningsen, S; Coxson, HO; McCormack, DG; Parraga, G; *Conventional non-contrast MRI of Ventilation Abnormalities in Bronchiectasis: New Tools and Measurements for an old Disease. Imaging Network of Ontario* 2014

11. **Paulin, G**; Svenningsen, S; Lewis, JF; McCormack, DG; Parraga, G; *Hyperpolarized ^{3}He MRI Ventilation Abnormalities of Cystic Fibrosis and Non-Cystic Fibrosis Bronchiectasis. Imaging Network of Ontario* 2014

LEADERSHIP and VOLUNTEER ACTIVITIES

09/11-08/12   **President**, Ivey School of Business Healthcare and Health Management Club
Richard Ivey School of Business, London, Ontario, Canada

09/10-08/11   **Section Rep**, Ivey School of Business Healthcare and Health Management Club Richard Ivey School of Business, London, Ontario, Canada

04/10   Leadership Education Program, Tiers 1 and 2
               The University of Western Ontario, London, Ontario, Canada

PROFESSIONAL MEMBERSHIPS

2013-present   American Thoracic Society
               Student Member

2013-present   Canadian Thoracic Society
               Student Member